Antiviral Research 231 (2024) 106006

Contents lists available at ScienceDirect

Antiviral Research

journal homepage: www.elsevier.com/locate/antiviral

Identification of antibody-resistant SARS-CoV-2 mutants via N4-Hydroxycytidine mutagenesis

Priya Kumar [a], Xiaoxiao Zhang [b,c], Rahul Shaha [d], Maik Kschischo [b], Matthias Dobbelstein [a,e,*]

[a] Department of Molecular Oncology, Göttingen Center of Molecular Biosciences (GZMB), University Medical Center Göttingen, 37077, Göttingen, Germany
[b] Department of Mathematics and Technology, University of Applied Sciences Koblenz, 53424, Remagen, Germany
[c] Department of Informatics, Technical University of Munich, 81675, Munich, Germany
[d] Department of Molecular Enzymology, Göttingen Center of Molecular Biosciences (GZMB), University of Göttingen, 37077, Göttingen, Germany
[e] Max Planck Institute for Multidisciplinary Sciences, Am Fassberg 11, 37077 Göttingen, Germany

ARTICLE INFO

Keywords:
SARS-CoV-2
COVID-19
Coronavirus
Therapeutic antibodies
Bamlanivimab
Cilgavimab
Sotrovimab
Bebtelovimab
S2K146
S2H97
Molnupiravir
N4-hydroxycytidine (NHC)
mutagenesis
Next generation DNA sequencing
Soluble ACE2
Vesicular stomatitis virus
Pseudotype

ABSTRACT

Monoclonal antibodies targeting the Spike protein of SARS-CoV-2 are effective against COVID-19 and might mitigate future pandemics. However, their efficacy is challenged by the emergence of antibody-resistant virus variants. We developed a method to efficiently identify such resistant mutants based on selection from mutagenized virus pools. By inducing mutations with the active compound of Molnupiravir, N4-hydroxycytidine (NHC), and subsequently passaging the virus in the presence of antibodies, we identified specific Spike mutations linked to resistance. Validation of these mutations was conducted using pseudotypes and immunofluorescence analysis. From a Wuhan-like strain of SARS-CoV-2, we identified the following mutations conferring strong resistance towards the corresponding antibodies: Bamlanivimab – E484K, F490S and S494P; Sotrovimab – E340K; Cilgavimab – K444R/E and N450D. From the Omicron B.1.1.529 variant, the strongly selected mutations were: Bebtelovimab – V445A; Sotrovimab – E340K and K356M; Cilgavimab – K444R, V445A and N450D. We also identified escape mutations in the Wuhan-like Spike for the broadly neutralizing antibodies S2K146 – combined G485S and Q493R – and S2H97 – D428G, K462E and S514F. Structural analysis revealed that the selected mutations occurred at antibody-binding residues within the receptor-binding domains of the Spike protein. Most of the selected mutants largely maintained ACE2 binding and infectivity. Notably, many of the identified resistance-conferring mutations are prevalent in real-world SARS-CoV-2 variants, but some of them (G485S, D428G, and K462E) have not yet been observed in circulating strains. Our approach offers a strategy for predicting the therapeutic efficacy of antibodies against emerging virus variants.

1. Introduction

The COVID-19 pandemic persists despite extensive vaccination efforts and acquired immunity from previous infections (Abenavoli, 2024; del Rio and Malani, 2023). A significant contributing factor to the ongoing spread of SARS-CoV-2 is the emergence of virus variants with immune evasion properties (Carabelli et al., 2023).

Monoclonal antibodies targeting the Spike protein have been a cornerstone of SARS-CoV-2 therapy, representing the first successful targeted treatment during the pandemic (Corti et al., 2021; Focosi et al., 2022). By binding to the Spike protein, particularly the receptor binding domain (RBD, Spike residues 333–527 (Lan et al., 2020)), these antibodies prevent interaction with the receptor Angiotensin-Converting Enzyme 2 (ACE2), thus inhibiting virus entry and replication (Jackson et al., 2022; Scialo et al., 2020). However, as the COVID-19 pandemic progressed, mutations in the SARS-CoV-2 Spike protein led to reduced efficacy of several therapeutic antibodies, especially those targeting the receptor binding motif (residues 438–506), a portion of the RBD that often maintains ACE2 binding even when mutated (Cox et al., 2023; Lan et al., 2020; Starr et al., 2021a; Thomson et al., 2021). Such mutations can reduce or abolish the interaction between Spike and antibody while maintaining the binding of Spike to ACE2.

Despite the clinical successes of therapeutic antibodies (Chen et al., 2021b; Montgomery et al., 2022; Razonable et al., 2022), those targeting the receptor-binding motif, such as Bamlanivimab (LY-CoV555) (Cohen et al., 2021; Jones et al., 2021), Cilgavimab/EVUSHELD (Montgomery

* Corresponding author.
E-mail address: mdobbel@uni-goettingen.de (M. Dobbelstein).

https://doi.org/10.1016/j.antiviral.2024.106006
Received 22 March 2024; Received in revised form 31 August 2024; Accepted 12 September 2024
Available online 16 September 2024

et al., 2022; Zost et al., 2020), and Bebtelovimab (LY-CoV1404) (Westendorf et al., 2022), lost effectiveness against most newer variants (Cox et al., 2023; Iketani et al., 2022; Wang et al., 2023a). In contrast, antibodies targeting more conserved Spike epitopes, such as Sotrovimab (Gupta et al., 2021; Pinto et al., 2020), were more durable (Focosi et al., 2024). By November 2022, most therapeutic monoclonal antibodies were revoked of their emergency use authorization by the FDA, for diminishing efficacy against emerging Omicron subvariants (FDA, 2021, 2024), underscoring the ongoing challenge.

Broad-spectrum antibodies targeting highly conserved epitopes of the Spike protein were developed for inhibiting viral infection. S2K146 (Park et al., 2022) and S2H97 (Starr et al., 2021a) are notable examples. S2K146, an ACE2-mimicking antibody, targets the ACE2-binding site on the RBD, effectively neutralizing the Spikes of Omicron variants of SARS-CoV-2 and even the former SARS-CoV (Park et al., 2022). On the other hand, S2H97 targets a cryptic epitope termed site V (residues 353–357, 393–396, 426–430, 462–466, 514–521 (Starr et al., 2021a);), which is exposed only when the RBD is in the open conformation, and it neutralizes Spike proteins across the sarbecovirus subgenus (Starr et al., 2021a). Such antibodies hold a strong potential for therapeutic use for current and future variants of SARS-CoV-2.

Anticipating the efficacy of therapeutic antibodies against specific virus variants is crucial. However, testing each variant's susceptibility to antibody neutralization is impractical due to the sheer number of variants. Predicting neutralization based on sequence information alone could address this challenge. To achieve this, in vitro evolution of antibody-resistant virus variants can be helpful (Gal-Tanamy et al., 2008; Oladunni et al., 2021; Pandey et al., 2014). However, SARS-CoV-2 acquires mutations only slowly due to the proofreading activity of its RNA polymerase (Moeller et al., 2022; Robson et al., 2020), and this renders in vitro selection comparatively slow and cumbersome.

To expedite virus mutagenesis in vitro, we previously demonstrated the usefulness of N4-hydroxycytidine (NHC) (Zibat et al., 2023), the active compound of the drug Molnupiravir (Sheahan et al., 2020). When NHC is incorporated into virus RNA, it causes mutations through ambiguous base pairing, resulting in transitions between adenine and guanine or between cytosine and uracil (Kabinger et al., 2021). Culturing SARS-CoV-2 with NHC enabled rapid selection of variants resistant to an alpaca-derived single chain antibody (nanobody) (Zibat et al., 2023).

Here, we report the selection of SARS-CoV-2 variants resistant to FDA-approved therapeutic antibodies and broadly-neutralizing antibodies. We first generated virus pools derived from Wuhan-like or Omicron B.1.1.529 strains by NHC, and we selected antibody-resistant variants from these pools. Deep sequencing revealed characteristic mutations mediating resistance, which were confirmed through site-directed mutagenesis and pseudotype experiments. Structural analysis showed that these mutations occur at interfaces between the Spike protein and antibodies. Our study suggests that in vitro selection of antibody-escape mutants provides a catalogue of resistance-conferring mutations for each antibody and facilitates the prediction of therapeutic efficacy.

2. Results

2.1. Sequential mutagenesis and selection of SARS-CoV-2 Wuhan strain gives rise to antibody-specific resistance

To provide a baseline for antibody neutralization, we first incubated a Wuhan-like strain of SARS-CoV-2 (Stegmann et al., 2021), referred to as 'Wuhan' from here on, with human monoclonal antibodies that were previously approved for emergency use on COVID-19 patients, namely Bamlanivimab/LY-CoV555 (Jones et al., 2021), Sotrovimab/GSK4182136 (Pinto et al., 2020), and Cilgavimab/AZD1061/COV2-2130, which is therapeutically used in combination with Tixagevimab/AZ8895/COV2-2196 as EVUSHELD (Loo et al., 2022; Zost et al., 2020). The virus was exposed to serial antibody dilutions, followed by infection of Vero E6 cells. Immunofluorescence staining of the virus N protein revealed successful infection. Bamlanivimab and Cilgavimab neutralized the virus at concentrations of 50 and 167 ng/mL, respectively, whereas a higher concentration of Sotrovimab (between 500 and 1670 ng/mL) was required for neutralization. These results (Fig. S1 A) are largely in agreement with previous findings (Chen et al., 2021c; VanBlargan et al., 2022; Zost et al., 2020).

Next, we used near-neutralizing concentrations of each antibody for selection from pools of virus mutants. The virus was first passaged twice in the presence of 400 nM NHC to achieve mutagenesis in two independent virus pools. Subsequently, three passages were carried out with each of the pools and with each of the three antibodies at increasing concentrations (Fig. 1A). After each passage, the amount of virus used for the next infection was adjusted according to the virus RNA content in the supernatant, as determined by quantitative RT-PCR. After the final passage, the resulting virus pools were subjected to further analysis regarding antibody resistance and accumulation of mutations.

To characterize the degree of resistance obtained with each selection scheme, we incubated all selected virus pools with each of all three antibodies under study, at serial dilutions, followed by infection of cultured Vero E6 cells and immunofluorescence staining to detect infected cells. Each selection resulted in strong resistance against the same antibody, and even antibody concentrations of 5 μg/mL did not fully neutralize the virus from selected pools (Fig. 1B). In contrast, we observed little if any cross-resistance to antibodies that had not been used for selection. We therefore anticipated that each antibody selected a different set of virus mutants.

2.2. Characteristic spike mutations are selected by each therapeutic antibody

Next, we characterized each of the virus pools by deep sequencing, revealing a distinctive set of mutations within the Spike RBD (residues 333–527), selected by each of the antibodies. Of note, overlapping sets of mutations were obtained in two parallel but independent selections with the same antibody. The depth of sequencing also allowed us to determine the mutation frequencies within the pools (Fig. 2, Suppl. Table 1). By the final selection round, some of the mutations had frequencies approaching 100% for each selection, suggesting that most viruses had acquired resistance-conferring mutations.

Bamlanivimab most strongly selected the Spike mutation F490S – in one selection, this mutation was by far dominant even at the first passage, exceeding 80% of all sequences in the pool. In the other selection, the mutation E484K was found besides F490S. The mutation S494P emerged in the second passage of the selection at a lower percentage and became more dominant in the third passage. The mutations K529R and Q493R were seen transiently in the initial round and were decreasing in frequency subsequently (Fig. 2). In the context of resistance to Bamlanivimab, F490S and E484K are also the key Spike mutations reported in other studies (Choudhary et al., 2022; Focosi et al., 2022; Jensen et al., 2021). E484K, F490S, and S494P cause a 100-fold or greater in vitro resistance against Bamlanivimab (Focosi et al., 2022; Starr et al., 2021b).

In the case of Cilgavimab, the mutation N450D was dominant in the first selection, with only a small fraction containing the mutation K444 R/E. The other virus pool selected with this antibody mostly revealed K444 R/E, with N450D only transiently emerging (Fig. 2). K444 is crucial for Cilgavimab binding to Spike (Dong et al., 2021). Accordingly, K444R is an acquired resistance mutation in SARS-CoV-2 patients after tixagevimab-cilgavimab infusion (Vellas et al., 2022). The same mutation also reduces neutralization by immune sera elicited by SARS-CoV-2 vaccines (Wang et al., 2023b). Furthermore, a VSV-pseudotype assay compared Cilgavimab neutralization of the SARS-CoV-2-BA.2 and BA.2.3.20 Spike proteins, the latter carrying the RBD mutations K444R and N450D, among others; there, the BA.2.3.20 variant showed strong

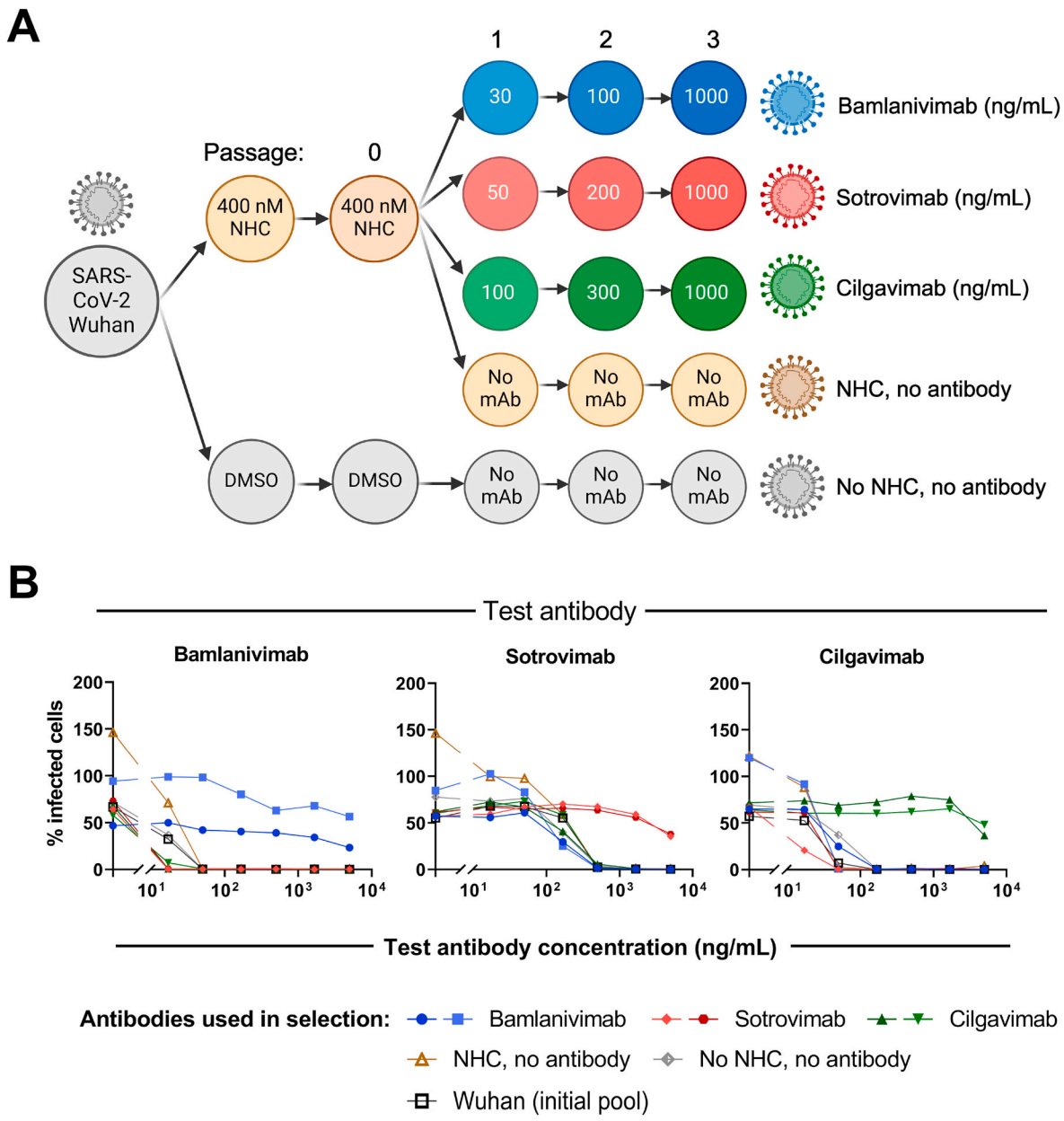

Fig. 1. Selection of antibody-resistant SARS-CoV-2 (Wuhan-like)

A. Sequential mutagenesis and selection. SARS-CoV-2 was first passaged twice through Vero E6 cells, in the presence of 400 nM NHC, to induce mutations within the virus genome. Subsequently, the pool of virus mutants was passaged through increasing concentrations of the indicated antibodies. After each passage, the virus RNA in the supernatant was quantified by RT-PCR, and the amount of virus used for the next inoculation was normalized accordingly. Mutagenesis and the selection with each antibody were performed in two independent replicates.

B. Acquired resistance of virus pools towards antibodies. Virus pools that had been selected by the indicated antibodies were used to infect a fresh monolayer of Vero E6 cells for 48 h at 37 °C, and the fractions of infected cells were determined by immunofluorescence analysis. Infections were performed in the presence of various concentrations of each of the three antibodies under study. This revealed the accumulation of strong resistance towards the same antibody that was used for selection, but no cross-resistance against the other antibodies.

antibody escape (Cao et al., 2023).

Sotrovimab yielded frequent mutations only after 2–3 passages of the mutant virus pool (Fig. 2). The mutation E340K became by far the most frequent in both selections. Remarkably, E340K was found distinctly in patients treated with Sotrovimab post SARS-CoV-2 Delta variant infection (Rockett et al., 2022) and has been associated with more than 297-fold increment in the Sotrovimab IC50 (Cathcart et al., 2022).

Some mutations occurred only transiently in the early passages – like Q493R with Bamlanivimab or V445A with Cilgavimab (Fig. 2) – and they were lost by the final passages as populations with other mutations became dominant. Still, Q493R and V445A are associated with decreased susceptibility of the virus to Bamlanivimab and Cilgavimab, respectively (Cao et al., 2023; Guigon et al., 2022).

When the mutant virus pool was passaged on Vero E6 cells, with or without antibody, mutations at R682 were always selected (Fig. S2). We have constantly obtained the same mutation in earlier selection experiments, too (Zibat et al., 2023). The mutation of R682 destroys a consensus site that is required for Furin-mediated pre-cleavage of the Spike for further activation by TMPRSS2-mediated cleavage (Hoffmann et al., 2020). Loss of the Furin cleavage site attenuates viral infectivity in human respiratory cell lines and animal models (Johnson et al., 2021; Peacock et al., 2021). However, in the TMPRSS2-deficient Vero E6 cells,

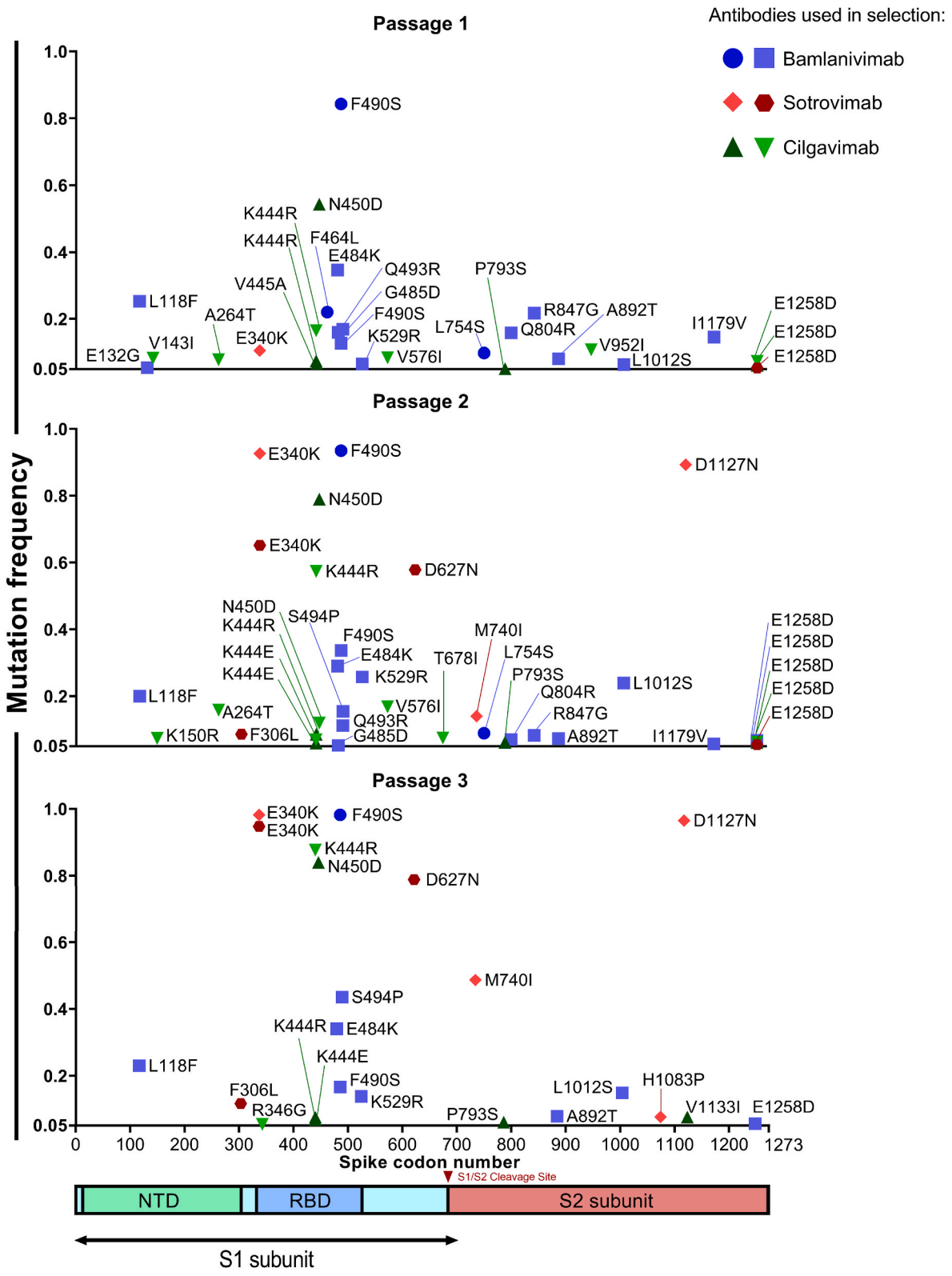

Fig. 2. Accumulated mutations within antibody-selected virus pools

After growing the Wuhan strain of SARS-CoV-2 in the presence of the indicated antibodies, the selected virus pools were subjected to deep sequencing (Suppl. Table 1, NCBI BioProject ID: PRJNA1143956) after each passage. Mutations with frequencies greater than 0.05 were plotted across the genomic sequence that encodes the Spike protein. Mutations within the receptor binding domain (RBD) accumulated at increased frequencies with each passage, and each antibody selected a characteristic set of amino acid exchanges. Mutations that were found when growing the virus both with and without antibody are shown in Fig. S2.

SARS-CoV-2 entry depends on cleavage by endosomal cathepsin B/L, such that the loss of the Furin cleavage site through R682 mutation does not hinder viral entry (Hoffmann et al., 2020). On the contrary, such mutations enhance infectivity towards Vero E6 cells (Johnson et al., 2021), perhaps by precluding the premature shedding of the S1 subunit (Peacock et al., 2021; Zhang et al., 2020).

To identify any antibody-selected mutations within the virus genome outside the Spike coding regions, we identified all mutations that accumulated in both selections carried out with each antibody at a frequency of at least 5%. A few conservative mutations fulfilling this criterion were found within the coding regions for NSP2, NSP3, NSP12, NSP16, ORF3a and N (Fig. S3). However, these mutations were all found with more than one antibody, and we also identified them in the initial NHC-treated virus pools and virus passaged without antibodies. Some of these mutations (NSP2: T85I, NSP12: P323L, ORF3a: Q57H, N: A381V) were already present in our initial Wuhan strain (Suppl. Table 1) as compared to the parental Wuhan strain (Stegmann et al., 2021), while we propose the others to be bystander mutations. Antibody-specific mutations were exclusively identified within the Spike coding region, suggesting that only such mutations confer strong resistance to antibodies.

2.3. Pseudotypes of vesicular stomatitis virus as well as immunofluorescence analyses confirm the impact of specific spike mutations on antibody-resistance

The selection of characteristic mutations with each antibody strongly suggests that these mutations abolish antibody-mediated neutralization. However, the selected virus pools were polyclonal in nature, and many of the individual viruses may carry additional mutations on top of the predominant Spike mutation. We therefore sought to clarify whether the most frequently selected mutations were individually sufficient to preclude neutralization by the corresponding antibodies. To test this, we generated expression plasmids for Spike mutants and used them to pseudotype a recombinant Vesicular Stomatitis Virus (VSV) that lacks its endogenous surface protein but expresses a green fluorescent protein (GFP) reporter (Zimmer et al., 2014). The pseudotyped VSVs were then assayed as to their capability of infecting Vero E6 cells, in the presence or absence of neutralizing antibodies. These assays revealed that each of the mutations that were strongly selected with each antibody was sufficient to confer near-complete resistance towards the same antibody (Fig. 3A). Again, however, we observed little if any cross-resistance towards antibodies that had not selected the same mutation (Fig. 3A). We conclude that each selected mutation is not only necessary but also sufficient to confer full resistance against the corresponding antibody.

Finally, we sought to determine whether the physical interaction of antibodies and Spike is actually prevented by single Spike mutations. Mutant Spike proteins were overexpressed in HeLa cells and visualized by immunofluorescence staining, using each therapeutic antibody as primary antibody and a fluorescence-labeled anti-human-IgG secondary antibody. Fluorescence microscopy and quantitative evaluation (Fig. 3B–C and Figs. S4–S6) revealed that the mutations – F490S, S494P and E484K; E340K; K444 E/R and N450D – strongly and highly significantly reduced the binding of the Spike protein to Bamlanivimab; Sotrovimab; and Cilgavimab, respectively.

2.4. Spike mutations map to antibody binding sites on spike structure models

To obtain insight into the structural basis of the mutations selected by each antibody, we mapped the most frequently selected mutations for each antibody to the structure of the Spike-RBD (Fig. 4A). For each antibody, the mutations clustered in distinct regions of the RBD, suggesting that they might locate at the RBD-antibody interface. We thus asked whether the mutations involved residues that contact the corresponding antibodies based on previous structure analyses, and this was indeed the case (Fig. 4B).

For instance, F490 of the RBD is essential for hydrophobic pi-stacking with the Y101 residue of Bamlanivimab heavy chain (Fig. 4B) (PDB structure 7l3n (Jones et al., 2021),), and this interaction is conceivably abolished by the F490S mutation. Similarly, E484 builds ionic interactions with the R50 residue of Bamlanivimab heavy chain based on opposite charges (Fig. 4B), and the mutation E484K is expected to destroy the interaction through exchanging a negative charge to a positive one. S494 of the RBD uses the backbone amide as a hydrogen donor to build a hydrogen bond with the E102 side chain of the Bamlanivimab heavy chain (Fig. 4B). Mutation of S494 to P presumably disrupts this interaction, since the nitrogen of P lacks a hydrogen ligand.

In the case of Sotrovimab (PDB structure 6wps (Pinto et al., 2020),), mutating the Spike E340 to K conceivably abolishes hydrogen bonds of the E residue with three amide groups of the peptide backbone within the antibody (residues 104–106, heavy chain) (Fig. 4B) by reverting the negative charge of E to the positive K residue. Loss of hydrogen bonds alone may not prevent antibody binding to the Spike protein, but when coupled with the steric hindrances introduced by the mutated amino acid, it is plausible that a single mutation could indeed preclude the binding of the antibody.

When interacting with the Cilgavimab heavy chain (PDB structure 7l7e (Dong et al., 2021),), the positively charged K444 of the Spike builds a combination of ionic interactions with the carboxyl group of D107 and hydrogen bonds with adjacent backbone-associated carbonyl groups (Fig. 4B). Furthermore, the amide of the N450 residue interacts with a carbonyl group of the antibody peptide backbone (Fig. 4B). Mutating these residues to acidic ones (K444E and N450D, respectively) plausibly destroys these interactions, whereas, the mutation K444R may introduce a steric clash with the interacting residues of Cilgavimab, due to the bulky guanidinium group on arginine. Most mutations found at lower frequency (e.g. Q493R, G485D, V445A) were also located near the epitope of the antibody (Dong et al., 2021; Jones et al., 2021).

To investigate whether the Spike mutants maintain viral infectivity and ACE2 binding, we prepared VSV-pseudotypes of wildtype and mutant Wuhan Spike proteins and infected Vero E6 cells to determine the levels of infection, comparing each mutant Spike relative to Wuhan Spike pseudotypes (set at 100%) (Fig. 4C). We observed that all Spike mutants, except E340K, showed similar or slightly higher infectivity compared to the wildtype. In a neutralization assay using soluble hACE2 (Fig. 4D), the Spike mutants E340K and K444E showed slightly reduced neutralization by hACE2 as compared to the Wuhan Spike. Thus, these Spike mutations affect ACE2 binding and virus infectivity only weakly if at all. This is consistent with the notion that selected viruses must still be capable of binding ACE2 for successful infection.

Taken together, we conclude that the mutations selected by passaging viruses in the presence of antibodies accumulated at residues located at the antibody binding sites. However, all mutations are still compatible with receptor binding and infection.

2.5. Sequential mutagenesis and selection of a SARS-CoV-2 omicron strain also results in antibody-resistance

We next investigated how an Omicron variant of SARS-CoV-2, B.1.1.529, could develop resistance to neutralization by antibodies, using a similar approach. Suppl. Table 2 shows the differences in the Spike sequence of this B.1.1.529 strain, compared to the Wuhan reference genome (NC_045512.2). This virus was passaged twice in NHC and then passaged separately in the presence of three antibodies – Bebtelovimab, Sotrovimab and Cilgavimab (Fig. 5A). Each of these antibodies were capable of neutralizing B.1.1.529. Bebtelovimab showed strong neutralization at 5 ng/mL, whereas Sotrovimab and Cilgavimab appeared weaker but still neutralized B.1.1.529 at 1.7 μg/mL and 5 μg/mL, respectively (Fig. S1 A). Bamlanivimab was ineffective (Fig. S1 A) and was, therefore, not used for resistance selection here. The observed neutralization capacities were in line with previous reports (Takashita

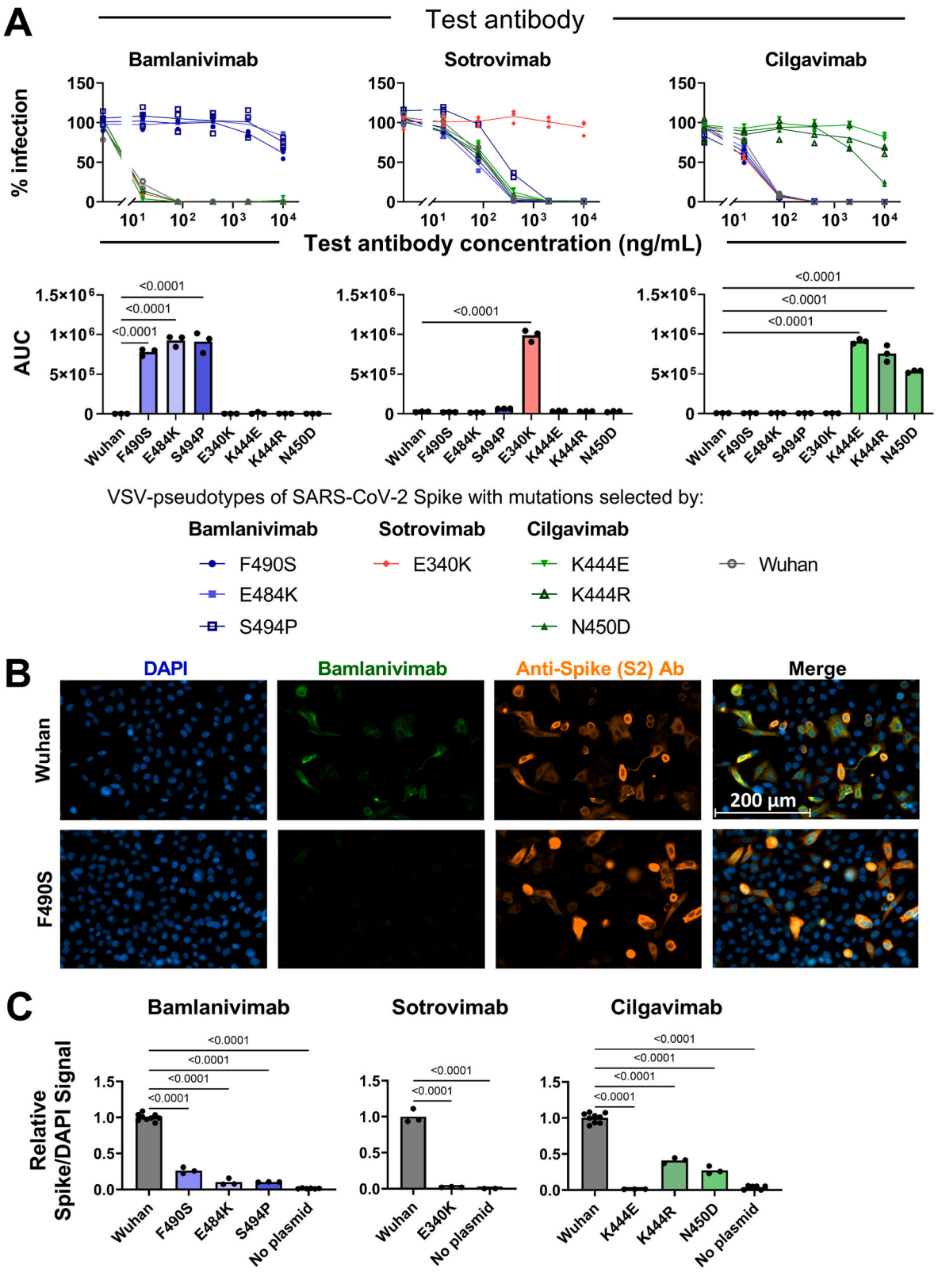

(caption on next page)

Fig. 3. Selected mutations diminish VSV-Spike-pseudotype neutralization and antibody binding
A. Antibody-mediated neutralization of wildtype and mutant Spike proteins displayed on VSV-pseudotypes. Spike proteins were incorporated into Vesicular Stomatitis Virus (VSV) pseudotypes, followed by infection of Vero E6 cells and quantification of the infected cells based on a GFP reporter contained in the recombinant VSV genome. The addition of antibodies revealed the degree of neutralization of each pseudotype. Each of the indicated point mutations was sufficient to confer near-complete resistance towards the antibody that it was selected by, but not towards the other antibodies. Each pseudotype-neutralization assay was performed in triplicate, and the individual results are displayed. Corresponding Dunnett's multiple comparison tests were performed with the areas under the curve (AUCs) to determine the significances of the indicated differences (adjusted p-values <0.05 indicated above each column).
B. Immunofluorescence staining to detect antibody-binding to wildtype and mutant Spike proteins in transfected HeLa cells. Spike proteins were overexpressed in HeLa cells by plasmid transfection for 48 h. The cells were fixed and immunostained with Bamlanivimab (5 μg/mL) and anti-Spike S2 (GTX632604, 1:2000) as primary antibodies, and anti-human-IgG coupled to the fluorescent dye AF488 (5 μg/mL) and anti-mouse-IgG coupled to AF546 (1:500) as secondary antibodies, along with DAPI (1:3000) for nuclear staining. The mutation F490S diminished the association of Bamlanivimab with the Spike protein. Analogous stainings for other mutant Spikes by Bamlaniviamb, Sotrovimab and Cilgavimab are shown in Suppl. Figs. S4–S6.
C. Quantification of the immunofluorescence signals. For each staining, the area covered by the AF488 signal above a specific threshold (indicating Spike bound to Bamlanivimab/Cilgavimab/Sotrovimab) was divided by the DAPI (nuclear) signal to obtain a Spike/DAPI ratio. The Spike/DAPI ratios were divided by the average Spike/DAPI ratio of wildtype Spike staining to obtain a relative Spike/DAPI signal ratio for each mutant Spike, wildtype Spike, and non-transfected HeLa cells. The binding of primary antibodies to corresponding mutant Spikes was significantly reduced compared to wildtype Spike (adjusted p-values <0.05 from Dunnett's multiple comparisons test indicated above each column).

et al., 2022; VanBlargan et al., 2022; Westendorf et al., 2022).

More passages were required for B.1.1.529 (Fig. 5A) than for Wuhan (Fig. 1A) to acquire antibody resistance. To assess whether the velocities of resistance acquisition generally differ, we passaged the Wuhan and B.1.1.529 strains in NHC and subsequently in Sotrovimab across four replicates. We observed that three out of four Wuhan virus pools had become resistant to Sotrovimab already after one passage, while only one of the B.1.1.529 replicates was mildly resistant but poorly infectious (Fig. S7 A). Hence, the Wuhan strain achieved resistance more quickly, perhaps due to its higher burst size (Fig. S7 B).

Upon selection with Bebtelovimab and Cilgavimab, virus pools were strongly resistant against their respective antibodies but also cross-resistant to the other antibody in the pair, suggesting that the virus pools had acquired overlapping sets of mutations (Fig. 5B). Sotrovimab-selected virus pools were resistant to Sotrovimab but not against the other two antibodies, predicting distinct mutations (Fig. 5B).

2.6. Each therapeutic antibody selects characteristic B.1.1.529 spike mutations

The B.1.1.529-derived resistant virus pools of passage 6 were deep-sequenced to identify the underlying mutations (Fig. 6, Suppl. Table 3). Both independent selections by Bebtelovimab accumulated the mutation V445A at almost 100% frequency. Previous pseudotype neutralization assays using the Wuhan Spike protein with V445A mutation result in significant reduction in susceptibility to Bebtelovimab (Westendorf et al., 2022).

With Sotrovimab, the E340K Spike mutation was selected in both independent selections of B.1.1.529 (Fig. 6), as in Wuhan (Fig. 2). In addition, the K356M mutation accumulated in one selection (Fig. 6). Interestingly, the E340K and K356*T* mutation also accumulated in patients infected with Omicron and treated with Sotrovimab (Birnie et al., 2022; Ragonnet-Cronin et al., 2023).

B.1.1.529 mutants passaged in Cilgavimab dominantly acquired the Spike mutation K444R in one selection and V445A in the other (Fig. 6), resembling the results of the Wuhan selection (Fig. 2). Unlike in Wuhan, however, the mutation N450D was only weakly selected along with K444R. The high overlap of mutations selected with Cilgavimab and Bebtelovimab readily explains the cross-resistance of selected pools (Fig. 5B).

The complex mutation E340D-V341D-F342L was detected at low frequencies in both independent selections for Bebtelovimab and in one selection each with Cilgavimab and Sotrovimab (Fig. 6). Since a similar set of mutations also accumulated without antibodies or NHC (Fig. S8, Suppl. Table 3), a low proportion of it might have been present in the initial virus preparation. Correspondingly, pseudotype assays with mutants that were built on the Omicron BA.1 Spike protein have previously revealed that E340D and V341*F* (not V341D) increased the EC50 values for Sotrovimab neutralization by > 609 and 5.9 times, respectively (FDA, 2023c). The presence of these mutations upon selection by Bebtelovimab and Cilgavimab may explain the mild cross-resistance of these pools against Sotrovimab (Fig. 5B).

As with all Wuhan-derived virus pools (Figs. S2 and S3), we observed a mutation at the Furin cleavage site, R685H, in single replicates of selection by Cilgavimab and Sotrovimab (Fig. 6). Notably, however, such mutations did not occur in the other selections or upon passaging of B.1.1.529 without antibody (Fig. S8, Suppl. Table 3), raising the question why the selection pressure towards such mutations seems less pronounced in B.1.1.529 than in Wuhan. Of note, the B.1.1.529 strain comprises the mutation P681H at the Furin cleavage site, as compared to the Wuhan Spike (Suppl. Table 2). This mutation decreases cleavage by host cell proteases and gives preference to entry through cathepsin rather than TMPRSS2 (Khatri et al., 2023; Willett et al., 2022), which is the preferred pathway in TMPRSS2-deficient Vero E6 cells (Hoffmann et al., 2020). This suggests that the B.1.1.529 mutation P681H decreases Spike cleavage, increases Omicron infectivity towards TMPRSS2-deficient cells and thus reduces the necessity of acquiring additional mutations at the adjacent sites R682 and R685.

2.7. Pseudotypes of vesicular stomatitis virus as well as immunofluorescence analyses confirm the impact of specific B.1.1.529 spike mutations on antibody-resistance

We used VSV-pseudotyped viruses displaying B.1.1.529 Spike proteins with single mutations to perform antibody neutralization assays. As in the Wuhan system, the selected mutations were sufficient to confer resistance against the corresponding antibodies (Fig. 7A). The mutation V445A, selected by both Bebtelovimab and Cilgavimab, provided complete resistance to both antibodies (Fig. 7A), largely explaining the cross-resistance observed between Bebtelovimab and Cilgavimab selected strains (Fig. 5B). The Sotrovimab-selected K356M mutation conferred remarkable resistance to the same but not different antibodies, with somewhat less impact than E340K. K444R and N450D mediated complete resistance against Cilgavimab, as did V445A. Interestingly, the mutation K444R, which was not selected by Bebtelovimab, also conferred complete resistance against this antibody, suggesting that K444 might contribute to binding Bebtelovimab as well.

Immunofluorescence staining of wildtype and mutant B.1.1.529 Spike proteins overexpressed in HeLa cells, similar to Fig. 3B–C, revealed that E340K and K356M diminished Sotrovimab staining (Fig. 7B–C; Fig. S5). Similarly, V445A reduced the staining intensity by Cilgavimab and Bebtelovimab (Fig. 7C; Figs. S9–S10); K444R and N450D also compromised the Cilgavimab-dependent fluorescence signal (Fig. 7C; Fig. S9). Hence, single mutations strongly and significantly reduced the ability of antibodies to bind the B.1.1.529 Spike protein.

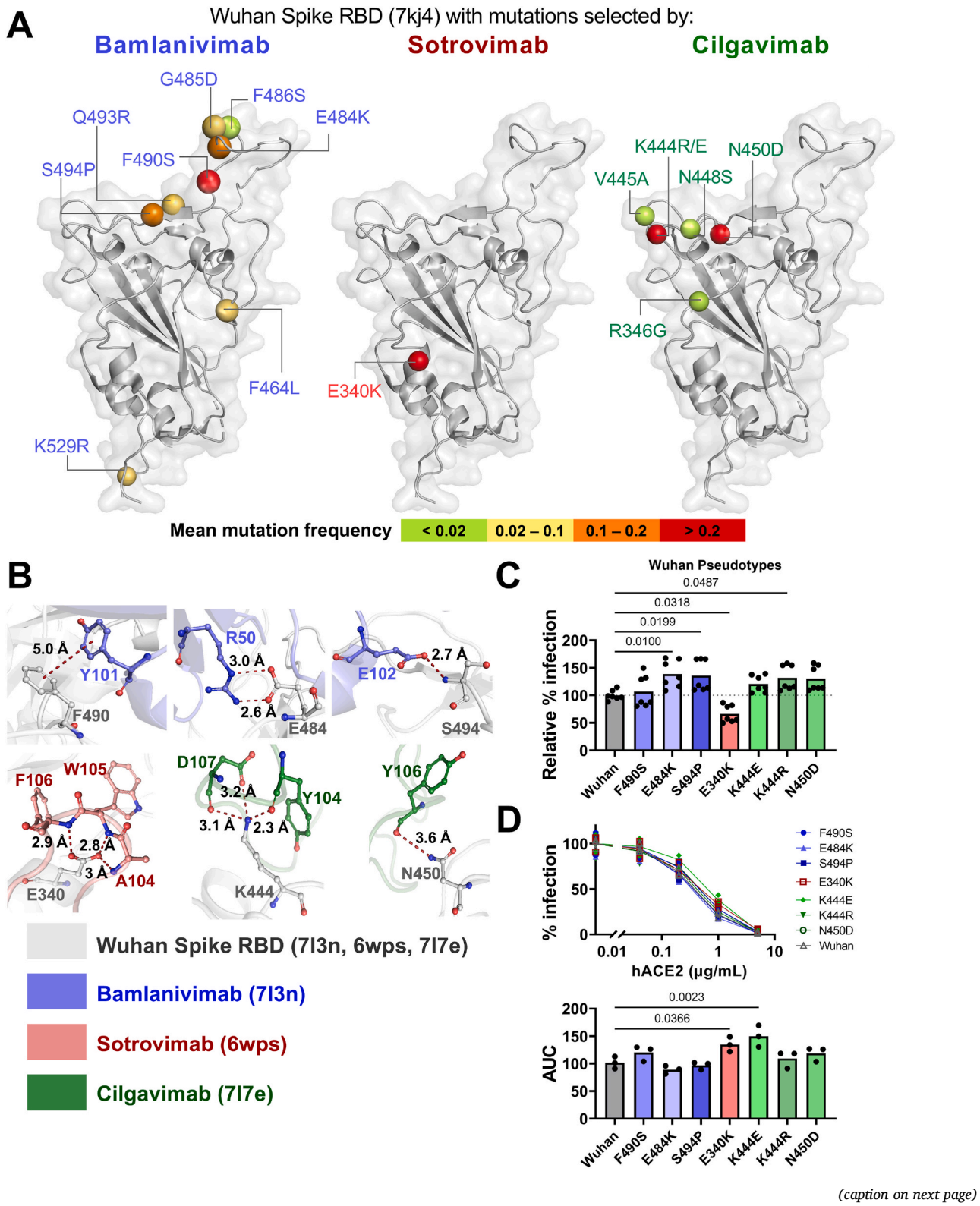

(caption on next page)

Fig. 4. Mapping of antibody-selected mutations on the three-dimensional structure of the Spike protein
A. Selected RBD mutations. The PDB structure 7kj4 (Xiao et al., 2021) was used to depict the location of mutations that were selected by Bamlanivimab, Sotrovimab or Cilgavimab. Displayed mutations occurred at a mean frequency (from the selection replicates) of >0.02 in at least one passage. The mean mutation frequencies (from both replicates and from all three passages) for each selecting antibody are color-coded on the Spike RBD (green: weakly selected mutations, red: strongly selected mutations). Mutations selected by each antibody indicate different epitopes for antibody-binding.
B. Interaction of mutated residues with antibodies. Bamlanivimab heavy chain interactions with Spike RBD residues F490, E484 and S494 were depicted on PDB structure 7l3n (Jones et al., 2021). The PDB structure 6wps (Pinto et al., 2020) was used to depict the Sotrovimab heavy chain and the interacting residue E340 of the Spike RBD. Cilgavimab heavy chain interactions with Spike RBD residues N450 and K444 were shown on 7l7e (Dong et al., 2021).
C. Impact of selected Spike mutations on pseudotype infectivity. VSV-pseudotypes with mutant Spike proteins were used to infect Vero E6 cells in parallel (n = 7). The infectivity was quantified by comparing the number of infected cells for each mutant to the average number of cells infected by VSV-pseudotypes with the wildtype Wuhan Spike, set at 100% (adjusted p-values <0.05 from Dunnett's multiple comparisons test indicated). The E340K Spike mutation markedly reduced the pseudotype infectivity.
D. ACE2-binding capacities of mutant Spike proteins. A pseudotype-hACE2 neutralization assay was conducted by incubating the VSV-pseudotypes of Spike mutants with increasing concentrations of soluble hACE2, followed by infection of Vero E6 cells overnight. The K444E and E340K mutants exhibited slightly reduced ACE2 binding compared to the wildtype Wuhan pseudotypes. Significances calculated through Dunnett's multiple comparisons test of the AUCs are shown in the lower graph.

2.8. Spike mutations map to antibody binding sites on B.1.1.529 spike structure models

We then mapped the most frequently selected mutations to the B.1.1.529 Spike RBD crystal structure (PDB structure 7wpc (Yin et al., 2022),) in Fig. 8A. Mutations selected by Bebtelovimab and Cilgavimab share similar clusters around residues 445–450, whereas Sotrovimab selected mutations around the subdomain at 340–356. Less frequent mutations around residue 340 (E340D-V341D-F342L) were also located there.

To predict interactions between Bebtelovimab and the B.1.1.529 Spike, the PDB structure 7mmo of Bebtelovimab bound to the Wuhan Spike (Westendorf et al., 2022) was modified by replacing the Wuhan Spike with the B.1.1.529 Spike from PDB structure 7wpc (Yin et al., 2022) through superimposition on PyMOL (Schrodinger, 2015). Accordingly, the positively charged K444 Spike residue forms ionic interactions with the negatively charged D56 of the Bebtelovimab heavy chain (Fig. 8B). This might be disrupted due to steric hindrance introduced by the K444R Spike mutation, thereby diminishing neutralization by Bebtelovimab (cf. Fig. 7A).

The PDB structure 7yad of Sotrovimab-bound Omicron Spike (Zhao et al., 2022) revealed polar interactions between the carboxyl group of E340 with backbone amides of A104 and W105 within the Sotrovimab heavy chain (Fig. 8B), conceivably abolished by the E340K mutation. On the other hand, the positively charged Spike residue K356 shows ionic interactions with the negatively charged E108 of the heavy chain, which could not be maintained upon the K356M mutation (Fig. 8B).

In a similar approach as for studying Bebtelovimab-B.1.1.529 Spike interactions, we superimposed the B.1.1.529 Spike from PDB structure 7wpc (Yin et al., 2022) onto Cilgavimab-bound Wuhan Spike in PDB structure 7l7e (Dong et al., 2021) (Fig. 8B). This strongly suggests that the positively charged Spike K444 interacts with the negatively charged D107 and the backbone carbonyl group at Y104 of the Cilgavimab heavy chain, as seen before with the Wuhan Spike (Fig. 4B). Lastly, the N450 residue on the B.1.1.529 Spike also displays polar interactions with the backbone carbonyl group of Y105 on Cilgavimab (Fig. 8B), and mutation N450D would disrupt this interaction.

At the position V445, which was frequently mutated upon selection by Bebtelovimab or Cilgavimab, the B.1.1.529 Spike is predicted to interact with residues of the two antibodies, but only through its peptide backbone (Fig. S11). Conceivably, the mutation V445A should not disrupt this interaction. However, previous reports also suggest that the mutation V445A confers resistance to both of these antibodies (Focosi and Casadevall, 2022; Haars et al., 2023), as we have observed (Fig. 7A–C). We speculate that the V445A mutation changes the flexibility of the Spike loop structure that comprises the V445 residue, thus precluding Bebtelovimab or Cilgavimab from binding.

Finally, we examined how the mutations selected in B.1.1.529 affected Spike infectivity (Fig. 8C) and hACE2-binding (Fig. 8D). E340K and K356M reduced B.1.1.529 Spike infectivity by approximately 50%, while the other mutations had no significant effect (Fig. 8C). Compared to the Wuhan Spike, the B.1.1.529 Spike showed stronger neutralization by hACE2, suggesting stronger hACE2 binding consistent with previous reports (Lupala et al., 2022; Shah and Woo, 2022) (Fig. 8D). Further, the E340K mutation was neutralized less effectively by hACE2 (Fig. 8D), suggesting that this mutation negatively affects Spike-ACE2 binding. This aligns with our earlier findings on the Wuhan-E340K mutant (Fig. 4D) and a previous study showing reduced ACE2 binding of E340K compared to wildtype Spike (Yi et al., 2021).

Hence, the mutations K444R and N450D contributed to Cilgavimab resistance on both Wuhan and B.1.1.529 Spikes. The mutation V445A on the B.1.1.529 Spike conferred resistance to both Cilgavimab and Bebtelovimab. The mutation E340K allowed Sotrovimab escape on both Wuhan and B.1.1.529 Spike proteins; however, this mutation also reduced the Spike infectivity and Spike-ACE2 binding, more strongly on the B.1.1.529 Spike than on the Wuhan Spike.

2.9. Sequential mutagenesis and selection of the SARS-CoV-2 Wuhan strain also results in resistance to broad-spectrum antibodies

To study the potential of developing resistance against antibodies targeting conserved epitopes of the Spike, we made use of two broadly-neutralizing antibodies (Fig. 9A) – S2K146 (Cameroni et al., 2022; Park et al., 2022), and S2H97 (Cameroni et al., 2022; Starr et al., 2021a). S2K146 and S2H97 completely neutralized the Wuhan strains at concentrations of 170 ng/mL and 10 μg/mL, respectively (Fig. S1 B). Yet, the antibodies neutralize through different mechanism. While S2K146 covers a surface of the RBD that largely coincides with the ACE2-binding region, S2H97 binds to a conserved epitope of the Spike largely outside the receptor-binding motif (Park et al., 2022; Starr et al., 2021a). Using a similar approach as described above, we passaged the Wuhan strain twice in 400 nM NHC and 3–4 times in increasing concentrations of the two antibodies across two replicates. By the third passage, we obtained virus strains that were completely resistant to S2H97 in both replicates (Fig. 9A). For S2K146, we observed partial resistance in only one virus pool (Fig. 9A). In the other virus pool, we failed to obtain virus resistant to S2K146 even after four passages. Interestingly, the Bamlanivimab-passaged virus strains tolerated slightly higher concentrations of S2K146 than the virus strains passaged with S2H97 or without any antibody (Fig. 9A).

We then subjected the genomes of the passaged virus pools to deep sequencing and plotted the mutated residues across the Spike gene, including frequencies greater than 0.05 (Fig. 9B–Suppl. Table 4, Fig. S12). Passaging in S2H97 strongly selected for the mutations D428G and S514F in one replicate and K462E in the other; at lower frequencies, the mutations E516K and L518Q appeared (Fig. 9B). For S2H97 (Starr et al., 2021a), deep mutational scanning has previously revealed mutations at residues 394, 396, 428, 462, 514, 516 and 518 to be relevant

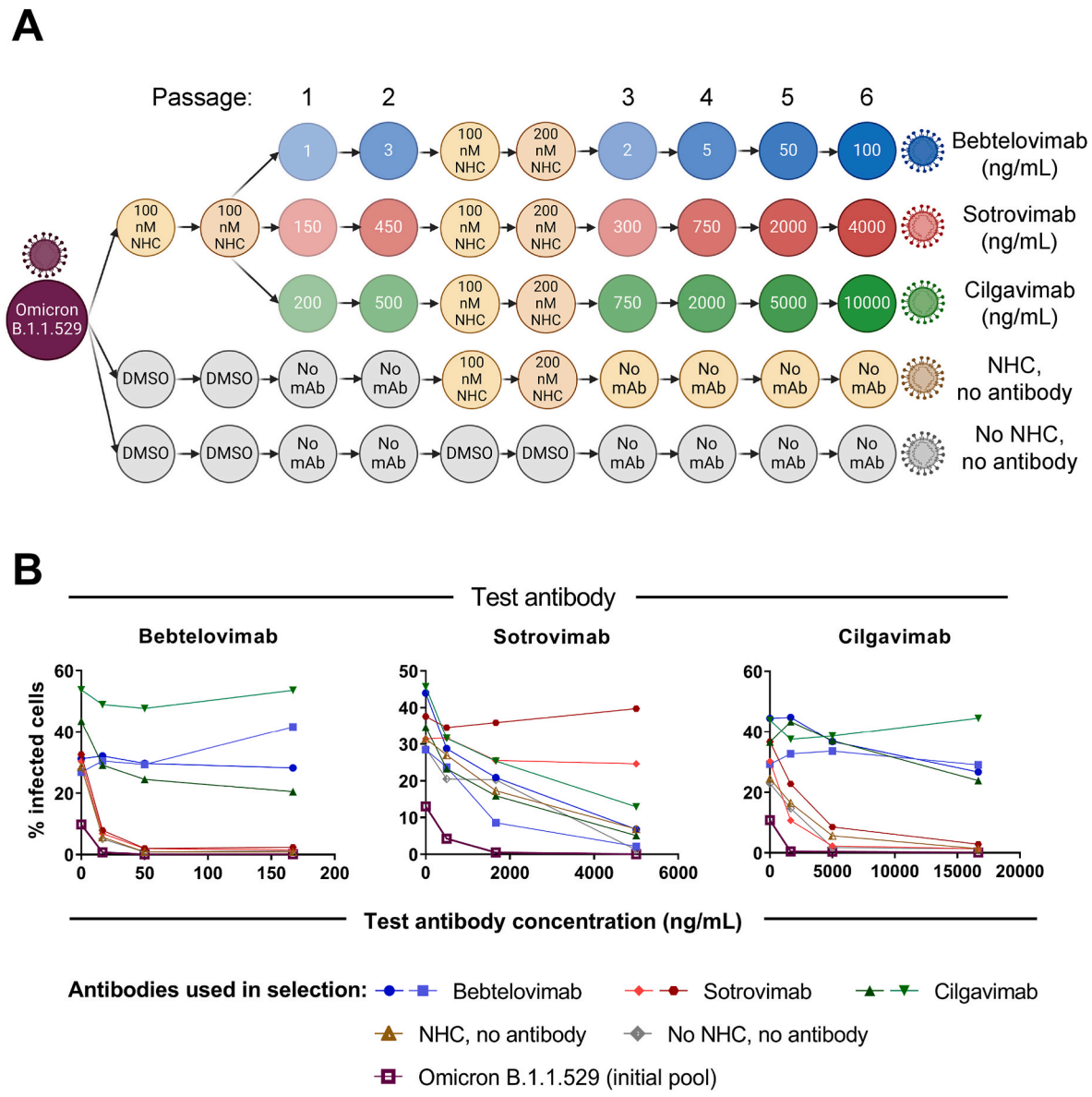

Fig. 5. Selection of antibody-resistant SARS-CoV-2, Omicron variant

A. Sequential mutagenesis and selection of Omicron B.1.1.529. Similar to the scheme in Fig. 1A, SARS-CoV-2 Omicron B.1.1.529 was passaged twice through Vero E6 cells in the presence of NHC, and then twice through increasing concentrations of the indicated antibodies. Two more mutagenesis steps were performed to increase the chances of attaining resistance, followed by four more passages with antibodies. For each antibody, two independent selections were carried out. In one replicate of the Bebtelovimab selection, the additional mutagenesis steps were omitted as remarkable resistance was already observed in passage 2 (Fig. S15).

B. Acquired resistance of SARS-CoV-2 Omicron B.1.1.529 towards antibodies. Analogous to Fig. 1B, selected B.1.1.529 pools in passage 6 were used to infect a Vero E6 monolayer at increasing antibody concentrations for 48 h. Immunofluorescence analyses showed high levels of resistance towards the selecting antibody in each case. Moreover, viruses selected with Bebtelovimab and Cilgavimab revealed strong cross-resistance to one another's antibody of selection, and low to moderate cross-resistance to Sotrovimab.

for antibody escape, with mutations at L518 providing the strongest resistance. Thus, the results of the previous and the current study largely overlap. One virus pool passaged in the presence of S2K146 had the mutations Q493R at close to 100% frequency and G485S at around 30% frequency, suggesting that Q493R and G485S co-exist in 30% of the population. The other replicate, which failed to develop resistance, had selected for Spike mutations S371F and D574N (Fig. 9B). In a prior study of S2K146, it was reported that, determined by deep mutational scanning assays, mutations at Spike residues 475, 484, 486, 487 and 489 reduce S2K146 binding (Park et al., 2022). These mutations are in the same area but do not coincide with the ones found here on the partially resistant virus pool. We propose that only the combination of two single mutations, Q493R and G485S, provided resistance towards S2K146.

2.10. Specific mutations confer resistance towards broad-spectrum antibodies, as confirmed by pseudotypes and immunofluorescence analyses

To confirm the impact of the major identified mutations on antibody resistance, we performed neutralization assays using VSV-pseudotypes of Wuhan Spike proteins with defined mutations occurring at frequencies greater than 0.2 in any replicate during antibody passaging (Figs. 9B and 10A). Among the single mutations selected by S2K146, the pseudotypes of mutants Q493R and S371F resulted in slightly more infection at 100 ng/mL S2K146 than the wildtype Wuhan Spike pseudotypes (Fig. 10A). The double mutant G485S + Q493R, however, was remarkably resistant to S2K146 (Fig. 10A). The Bamlanivimab-resistant mutation E484K also showed mild resistance to S2K146 at 100 ng/mL.

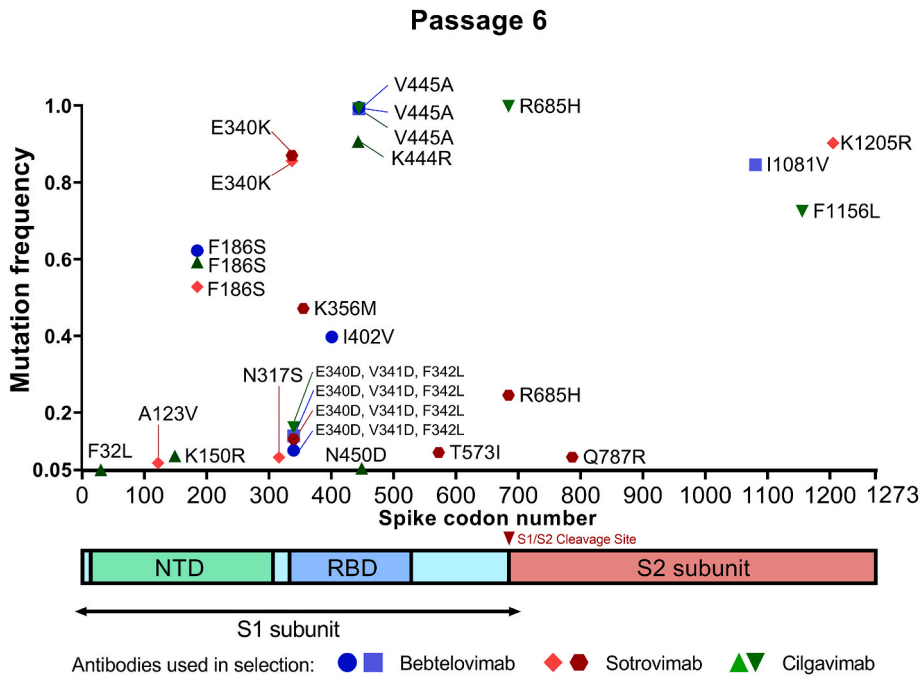

Fig. 6. Mutations conferring resistance of SARS-CoV-2 Omicron B.1.1.529 towards antibodies
Upon passaging NHC-treated B.1.1.529 with antibodies, the selected virus pools were subjected to deep sequencing (Suppl. Table 3, NCBI BioProject ID: PRJNA1143956) after the sixth passage. Mutations with frequencies greater than 0.05 were plotted across the genomic sequence that encodes the Spike protein. As for Wuhan (Fig. 2), frequent mutations were identified within the receptor binding domain (RBD). Mutations that occurred both in the absence and in the presence of antibodies are omitted here and displayed in Fig. S8.

All three mutations selected by S2H97 resulted in strong resistance to S2H97, and surprisingly, S371F (selected by S2K146) also conferred resistance to S2H97 (Fig. 10A).

In an immunofluorescence staining assay similar to Fig. 3B–C and Fig. 7B–C, we observed that all mutations selected by S2H97 resulted in significant loss of the Spike signal as compared to the wildtype Wuhan Spike (Fig. 10B–C, Fig. S13). The single mutations selected by S2K146 (except D574N) resulted in moderate loss of the Spike signal (Fig. 10C; Fig. S14). However, the double mutant G485S + Q493R completely eliminated Spike detection by S2K146 (Fig. 10C; Fig. S14). These results align well with the pseudotype neutralization assay, confirming the partial or full resistance conferred by each mutation. Importantly, the single mutations found upon selection by S2K146 were insufficient for antibody escape in a pseudotype assay or in an antibody-binding assay, whereas mutations at residues 485 and 493 together conferred a strong degree of resistance. Thus, even the broadly active antibody S2K146 can give rise to resistant virus strains, but the requirement for two simultaneous mutations probably reduces the velocity of resistance formation.

2.11. Spike mutations map to broad-spectrum antibody binding sites for S2K146 and S2H97

We mapped the frequently selected mutations onto the previously reported crystal structures of the antibody-Spike-complexes (Fig. 11A). Among the mutations strongly selected by S2K146, two locate in the corresponding epitope (Q493R and G485S) on the Spike RBD (PDB 7tas (Park et al., 2022),). The mutations selected with S2H97 cluster in the antibody-binding region outside the receptor-binding motif (but still within the RBD), around residues 428 and 518 (PDB 7m7w (Starr et al., 2021a),).

Detailed structural analysis of the Spike protein bound to S2K146 in the 7tas structure (Park et al., 2022) revealed that G485 is involved in polar interactions between its backbone carbonyl and amide group and W105 of the S2K146 heavy chain (Fig. 11B). Q493, on the other hand, forms ionic interactions with H32 and the backbone carbonyl group of L100 of the S2K146 heavy chain. The Q493R mutation likely introduces steric hindrance, while G485S may restrict antibody binding by decreasing the loop flexibility. For the residues mutated with high frequency upon passaging with S2H97, all are present at antibody contact sites (7m7w (Starr et al., 2021a),). D428 (Spike) displays an ionic interaction with H102 (antibody heavy chain); furthermore, K462 interacts with D55 and D57 of the S2H97 heavy chain, while S514 engages in non-polar interactions with Y103 of the heavy chain (Fig. 11B). Therefore, mutations at these residues explain direct interferences in antibody binding through the loss of molecular interactions as well as steric and charge-based clashes.

Finally, we assessed the effects of mutations at conserved sites on the Spike on viral infectivity and ACE2 binding (Fig. 11C–D). We observed that all studied Spike mutants, except K462E, resulted in a decrease in infectivity, with the S371F mutant attenuating infectivity the most. K462E appeared to improve infectivity. In a neutralization assay using soluble hACE2 (Fig. 11D), we observed that K462E was the only mutant more susceptible to hACE2 neutralization than the non-mutated Wuhan Spike. The double mutant G485S + Q493R and the mutant D428G showed slightly reduced neutralization by hACE2, whereas the S371F mutant was not neutralized by hACE2 at all, indicating a strong loss of ACE2 binding, which correlates with its poor infectivity (Fig. 11C). S371F was shown previously to decrease infectivity in VSV pseudotypes (Pastorio et al., 2022).

Overall, our results show that SARS-CoV-2 can acquire resistance against antibodies that target conserved sites, sometimes at the cost of reduced infectivity and decreased ACE2 binding. However, the mutation K462E is a notable exception that not only confers complete resistance to S2H97 but also increases Spike infectivity and ACE2 binding. Therefore, this mutation is of particular concern for surveillance. Finally, the virus largely remains susceptible to antibodies like S2K146 that strongly overlap with the highly conserved ACE2 binding sites, unless it accumulates a combination of mutations – thus, we propose that such antibodies should be prioritized for therapeutic strategies.

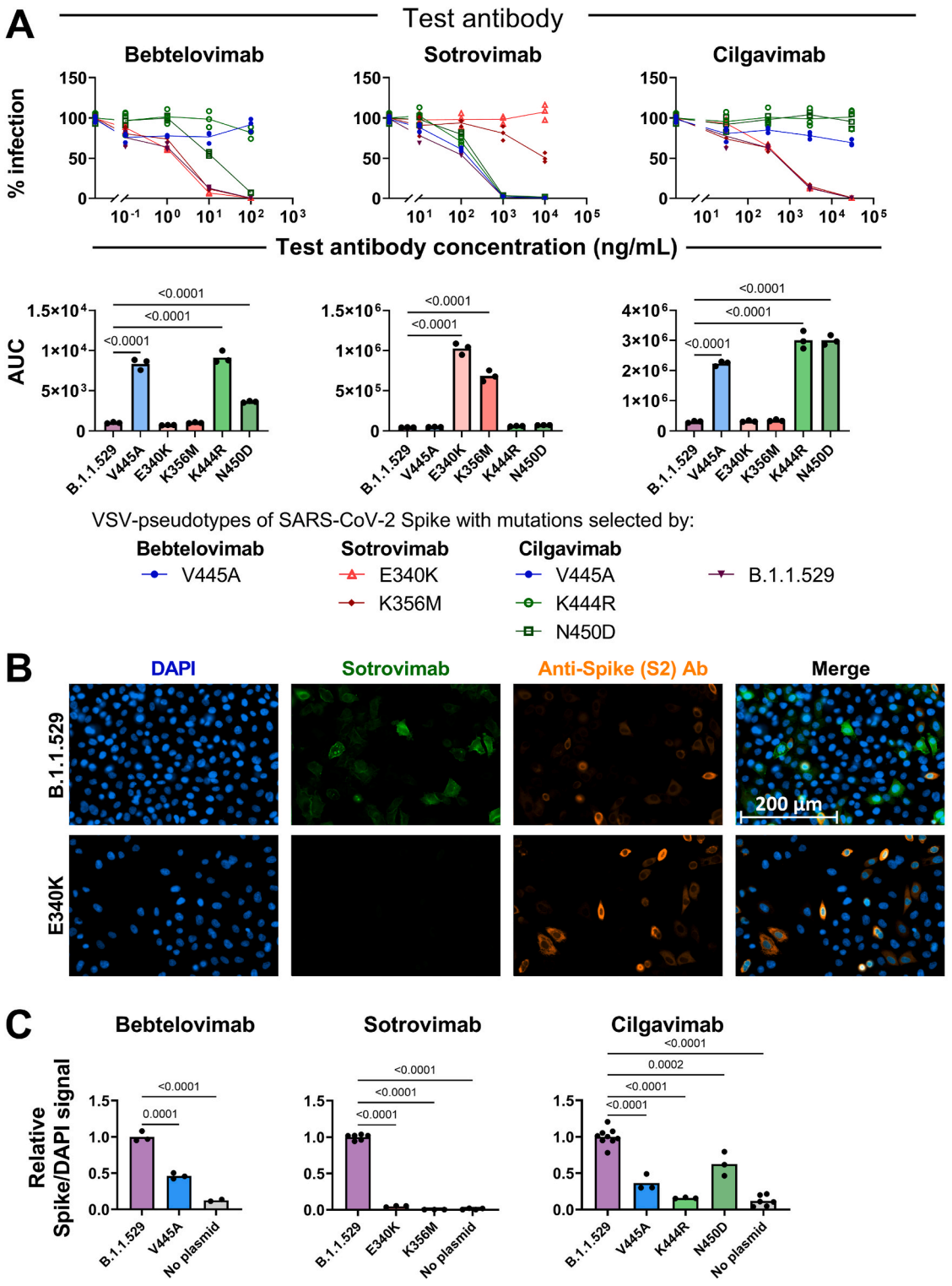

Fig. 7. Selected-B.1.1.529 Spike mutations diminish neutralization and binding by antibodies

A. Neutralization of VSV-pseudotypes containing wildtype or mutant B.1.1.529 Spike protein. As performed in Fig. 3A, VSV-pseudotypes of B.1.1.529 and mutant Spike proteins were used to infect Vero E6 cells, after incubations in antibodies at different dilutions. The indicated point mutations on their own were capable of conferring resistance to the antibody they were selected with. Dunnett's multiple comparisons tests were performed on the corresponding AUCs and the adjusted p-values <0.05 are displayed. Mutations K444R and V445A conferred resistance to both Bebtelovimab and Cilgavimab.

B. Immunofluorescence staining to detect antibody-binding to B.1.1.529 and mutant Spike proteins in transfected HeLa cells. Similar to Fig. 3B, we performed immunostaining of mutant and wildtype B.1.1.529 Spike proteins overexpressed in HeLa cells. When using Sotrovimab (5 µg/mL) for staining the B.1.1.529 Spike and its E340K mutant, the staining of the latter is reduced. Figs. S5, S9, S10 show immunostaining for other B.1.1.529 mutations with Sotrovimab, Cilgavimab and Bebtelovimab.

C. Quantification of the immunofluorescence signals. As in Fig. 3C, relative Spike/DAPI signal ratios were plotted for mutant Spike, B.1.1.529 Spike and untransfected HeLa cells. The binding of primary antibodies to corresponding mutant Spikes is significantly reduced compared to wildtype B.1.1.529 Spike (for significant differences, adjusted p-values from Dunnett's multiple comparisons test are mentioned).

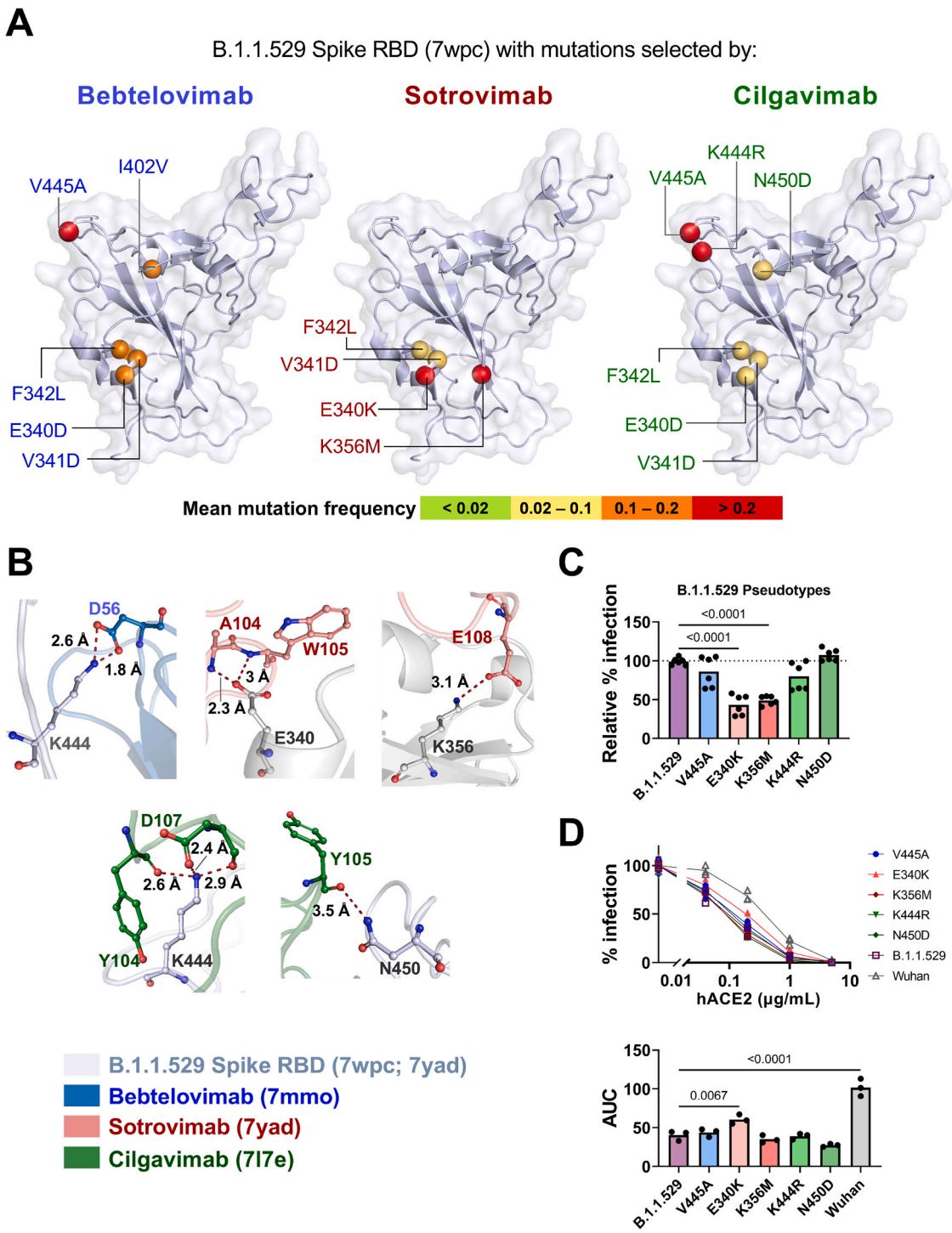

Fig. 8. Mapping of antibody-selected mutations on the three-dimensional structure of the B.1.1.529 Spike protein

A. Locations of mutations. Similar to Fig. 4A, the mutations that were selected by Bebtelovimab, Sotrovimab and Cilgavimab were mapped on the B.1.1.529 Spike structure PDB 7wpc (Yin et al., 2022).

B. Contact sites of antibodies and the B.1.1.529 RBD. The interaction of the Bebtelovimab heavy chain with the B.1.1.529 Spike RBD at residue K444 was displayed by superimposing the structure of the antibody with Wuhan Spike, according to PDB 7mmo (Westendorf et al., 2022), with the B.1.1.529 Spike (PDB 7wpc). PDB structure 7yad (Zhao et al., 2022) was used to depict the Sotrovimab heavy chain and B.1.1.529 Spike RBD interacting residues E340 and K356. The interactions of the Cilgavimab heavy chain with B.1.1.529 Spike RBD residues K444 and N450 were derived from a superimposition as for Bebtelovimab and indicated based on PDB 7l7e (Dong et al., 2021) and 7wpc (Yin et al., 2022).

C. Impact of selected Spike mutations on pseudotype infectivity. Vero E6 cells were infected with VSV-pseudotypes of the B.1.1.529 Spike and its mutants (n = 6). The infection rates were measured as percentages relative to the wildtype B.1.1.529 pseudotype, as described in Fig. 4C. The E340K and K356M mutations in the Spike protein led to a ~50% reduction in pseudotype infectivity (adjusted p-values <0.05 from Dunnett's multiple comparisons test indicated).

D. ACE2-binding capacities of mutant Spike proteins. An ACE2-pseudotype neutralization assay was performed using VSV-pseudotypes with wildtype and mutant B.1.1.529 Spike proteins, as outlined in Fig. 4D. The E340K Spike mutation remarkably reduced ACE2 binding, as shown in the AUC comparisons (adjusted p-values <0.05 from Dunnett's multiple comparisons test mentioned).

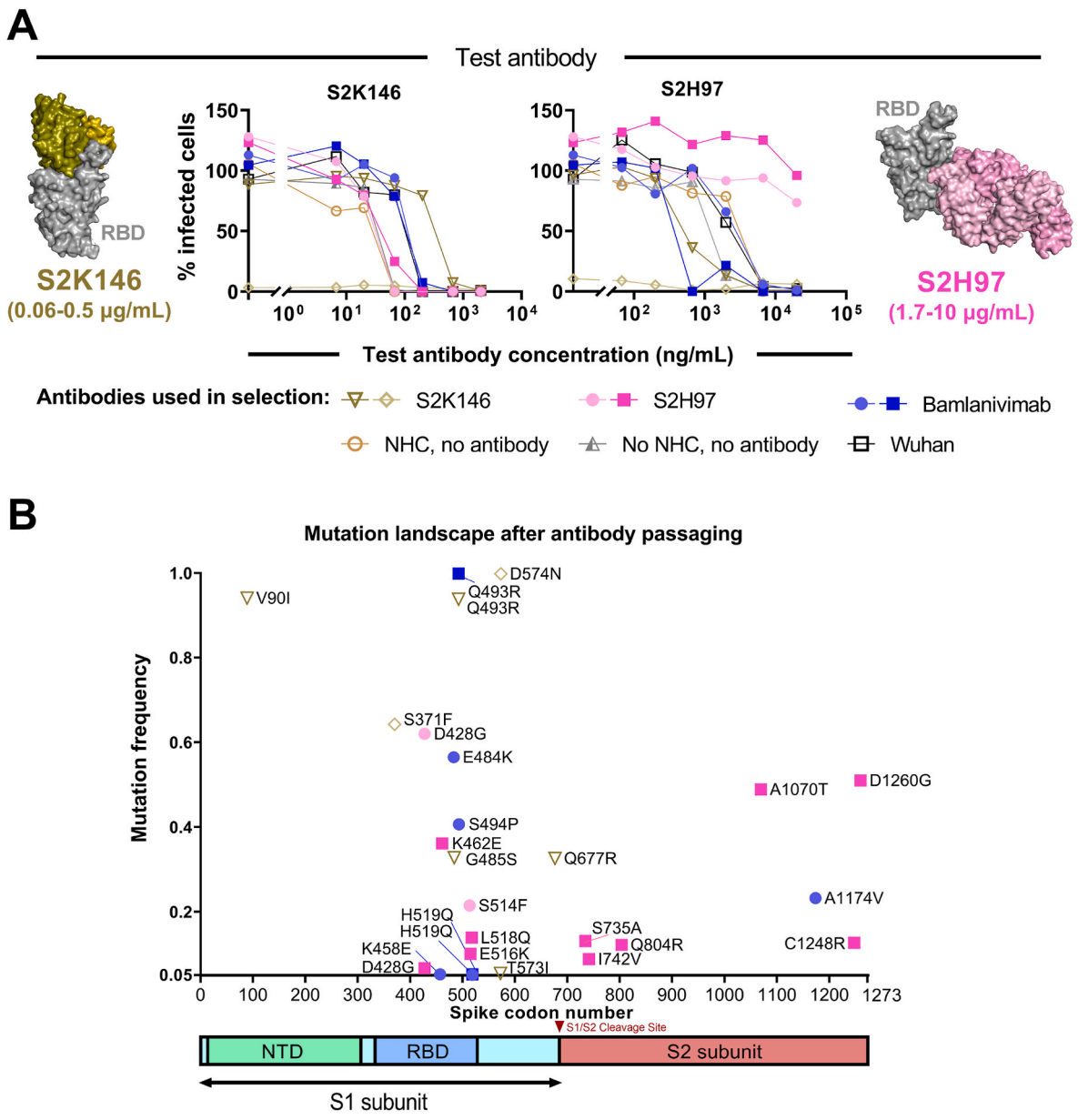

Fig. 9. Selection of SARS-CoV-2 Wuhan mutants resistant to broadly neutralizing antibodies

A. Selection of SARS-CoV-2 mutants that are partially or fully resistant to broad-spectrum antibodies targeting conserved epitopes of the RBD. S2K146 (PDB 7tas (Park et al., 2022),) binds to an epitope largely overlapping with the ACE2 binding epitope, while S2H97 (PDB 7m7w (Starr et al., 2021a),) binds to a cryptic epitope termed site V (residues 353–357, 393–396, 426–430, 462–466, 514–521) (Starr et al., 2021a). The Wuhan strain of SARS-CoV-2 was passaged twice in NHC and thrice in increasing concentrations of the referred antibodies (range mentioned), similar to the method in Fig. 1A. An additional virus pool was also passaged in Bamlanivimab as in Fig. 1A for comparison. The third passages of the virus pools were tested for resistance against the antibodies, as described in Fig. 1B. Partially resistant mutants were selected with S2K146, while fully resistant strains emerged with S2H97. Note that one of the S2K146-selected replicates was passaged four times and the resulting virus pool was not infectious, likely due to the S371F mutation (cf. Fig. 9B)

B. Mutations identified from deep sequencing of the selected virus pools. The genomes of resistant virus pools were sequenced (Suppl. Table 4, NCBI BioProject ID: PRJNA1143956), and mutation frequencies >0.05 were plotted across the Spike-encoding region of the SARS-CoV-2 genome. High frequency mutations characteristic to each tested antibody appeared within the RBD. The mutations Q493R and G485S were co-selected with S2K146 in one replicate. Mutation at site R682 occurred frequently in all samples but was excluded from the plot (cf. Suppl. Table 4). Mutations occurring in control samples passaged without antibody are shown in Fig. S12.

2.12. Some but not all of the selected resistance-conferring mutations are found in previously emerged major SARS-CoV-2 variants of concern

Finally, we compared the most frequently selected Spike mutations from our experiments with the SARS-CoV-2 variants that had emerged during the pandemic. As shown in Table 1, most of these mutations are indeed contained within such variants (ECDC, 2024; GISAID, 2024; NCBI, 2023). This explains why Bamlanivimab and Cilgavimab (used in combination with Tixagevimab as Evusheld) are no longer capable of neutralizing the most recent virus variants and have thus lost approval by the FDA (FDA, 2021, 2023a), in agreement with previous reports (Brady et al., 2022; Hoffmann et al., 2021; Jensen et al., 2021; Keam, 2022). In contrast, mutations at E340 do not occur in patients with high frequency yet, and this provides a rationale why Sotrovimab was still successfully used for treating Omicron BA.1 (Cameroni et al., 2022; FDA, 2023c; Iketani et al., 2022). So far, E340K has only been found in a

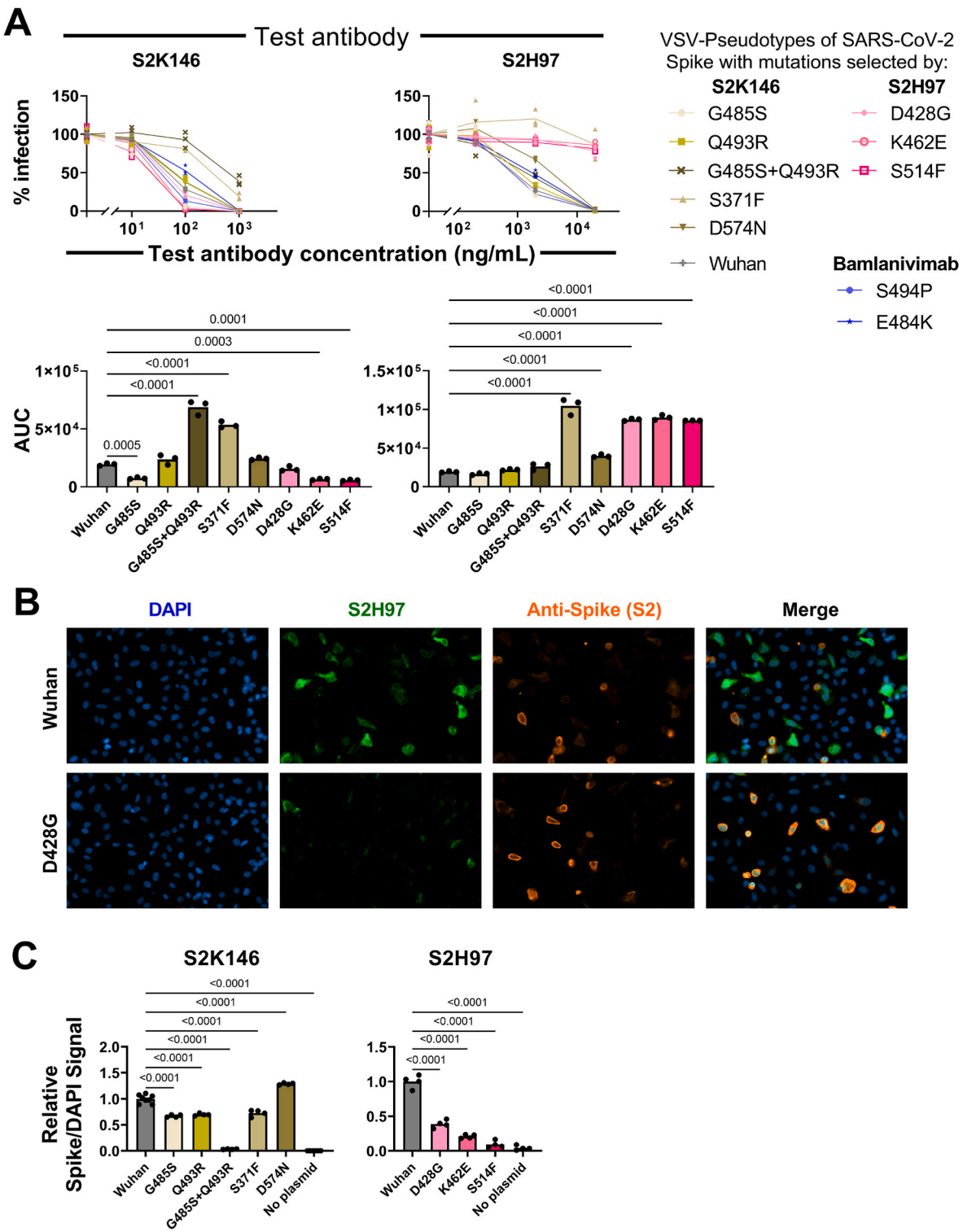

Fig. 10. Pseudotype assays and immunofluorescence staining to determine the extent of antibody binding to wildtype or mutant Spike proteins

A. VSV-pseudotype neutralization assay at increasing antibody concentrations indicated single mutations that confer antibody resistance. Wildtype or mutant Spike proteins were displayed on VSV-pseudotypes and used in an antibody-neutralization assay as described in Fig. 3A. The infection levels were normalized to wells without antibodies, with each mutation tested in triplicate. Corresponding AUCs with adjusted p-values <0.05 are shown in the lower graphs.

B. Immunofluorescence staining to show diminished antibody binding to mutant Spike proteins. As described in Fig. 3B, HeLa cells overexpressing wildtype or mutant Spike proteins were fixed and stained with the corresponding antibodies which selected the mentioned mutations. These antibodies were visualized by secondary anti-human antibodies coupled to the fluorescent dye AF488. When comparing the staining of Wuhan Spike and its mutant D428G by S2H97 (2 μg/mL), the staining of S2H97 was attenuated. Figs. S13 and S14 show immunostaining for other Wuhan mutations with S2H97 and S2K146, respectively.

C. Quantification of immunofluorescence signals. Spike signals obtained by individual antibodies were divided by the DAPI signal and normalized by the Spike/DAPI ratio for the Wuhan Spike, as described in Fig. 3C. S2H97-selected mutants showed significant reductions in staining. In contrast, single mutants obtained by selection with S2K146, apart from D574N, gave rise to a moderately reduced signal. The double mutant G485S + Q493R completely abolished binding to S2K146. All adjusted p values are <0.0001 (Dunnett's multiple comparisons test).

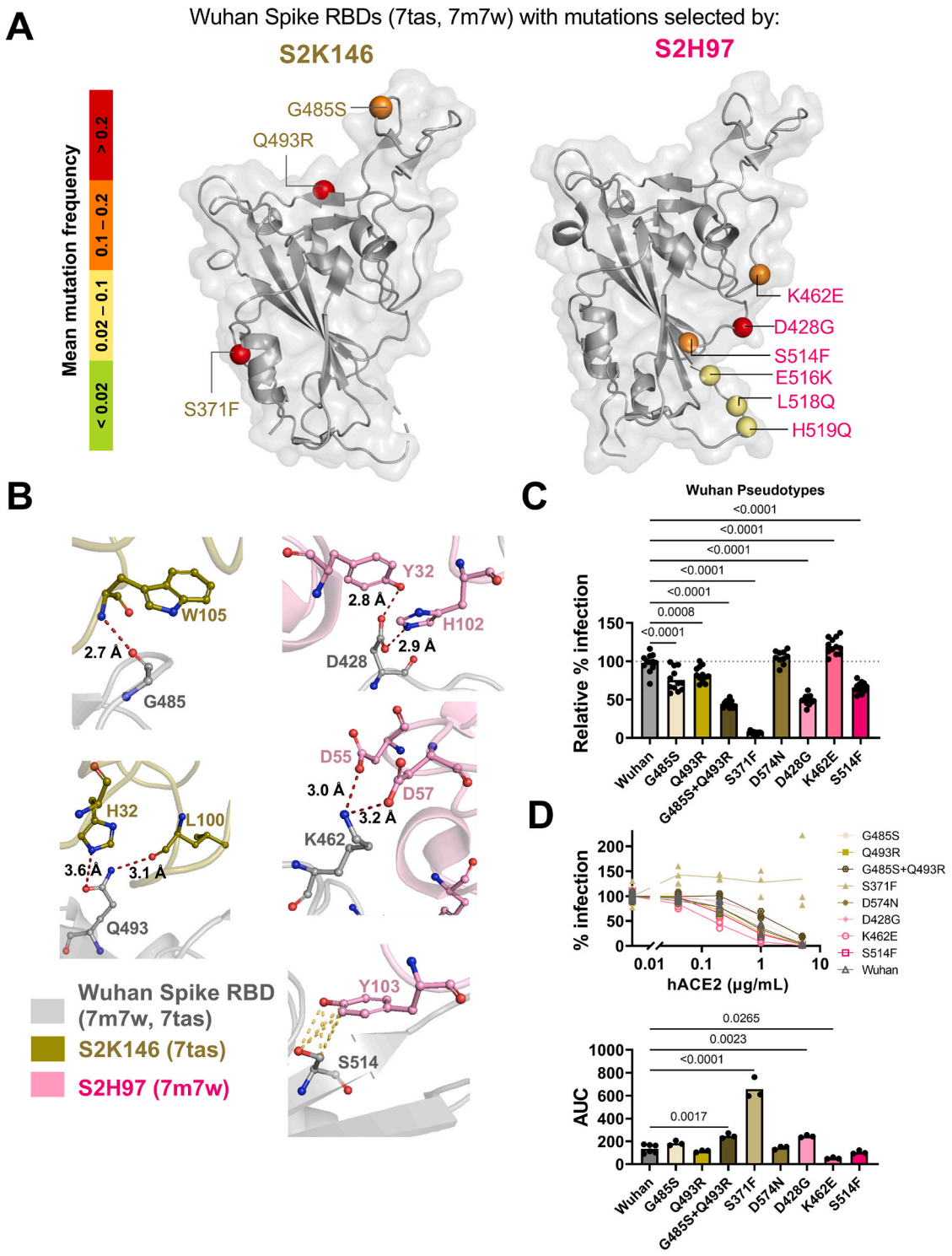

Fig. 11. Mapping of selected mutations on the structures of the Spike RBD

A. Locations of mutations. The residues mutated upon selection with S2K146 and S2H97 are displayed on the Wuhan Spike structures from PDB 7tas (Park et al., 2022), and PDB 7m7w (Starr et al., 2021a), respectively, using the same criterion and color code as described in Fig. 4A. Low frequency complex mutations at residues E340, V342, and F343 were observed in both selections, as well as in the absence of antibody passaging and the initial Wuhan strain (Suppl. Table 4); thus, they were omitted.

B. Contact sites of antibodies and the Wuhan RBD. Interaction between the studied residues mutated upon S2K146 selection and S2H97 selection were visualized on PDB structures 7tas (Park et al., 2022) and 7m7w (Starr et al., 2021a), respectively. The Spike residues are involved in direct interactions with S2K146 and S2H97.

C. Impact of selected Spike mutations on pseudotype infectivity. Relative infection efficiencies of VSV-pseudotypes with mutant Spike proteins were assessed as described in Fig. 4C (n = 12). Most mutations, except K462E, reduced infectivity, with S371F causing the greatest reduction (significant differences indicated with adjusted p-values <0.05).

D. ACE2-binding capacities of mutant Spike proteins. VSV-pseudotypes of wildtype and mutant Spikes (Wuhan) were used in ACE2-neutralization assays, as outlined in Fig. 4D. The Spike mutation K462E increased binding to soluble hACE2, while S371F, G485S + Q493R, and D428G reduced hACE2 binding as determined by AUC comparisons in the lower plot (adjusted p-values <0.05 indicated).

Table 1
Occurrence of selected Spike mutations in previously isolated SARS-CoV-2 variants.

WHO label	Lineage + additional mutations	Key Spike mutations (within residues 330-681) Colours indicate mutations selected by Bamlanivimab, Sotrovimab, Cilgavimab, Bebtelovimab, S2K146, and S2H97											Status (as of 26 July, 2024)
Omicron	BA.2.86	I332V	G339H	K356T	**S371F**	S373P	S375F	T376A	R403K	D405N	R408S	K417N	Variants of Interest
		N440K	V445H	G446S	**N450D**	L452W	N460K	S477N	T478K	N481K	**E484K**	F486P	
		Q498R	N501Y	Y505H	E554K	A570V	D614G	P621S	H655Y	N679K	P681R		
Omicron	KP.3	I332V	G339H	K356T	**S371F**	S373P	S375F	T376A	R403K	D405N	R408S	K417N	
		N440K	V445H	G446S	**N450D**	L452W	L455S	F456L	N460K	S477N	T478K	N481K	
		del483/483	**E484K**	F486P	Q493E	Q498R	N501Y	Y505H	E554K	A570V	D614G	P621S	
		H655Y	N679K	P681R									
Omicron	BA.2.86 + R346T + F456L	R346T	F456L										Variants under Monitoring
Omicron	BA.2.86 + R346T	R346T											
Omicron	BA.2.86 + F456L	F456L											
Alpha	B.1.1.7+E484K	**E484K**	N501Y	A570D	D614G	P681H							De-escalated Variants
n/a	B.1.214.2	Q414K	N450K	D614G									
n/a	B.1.1.7+S494P	**S494P**	N501Y	A570D	D614G	P681H							
Lambda	C.37	L452Q	**F490S**	D614G									
Beta	B.1.351	K417N	**E484K**	N501Y	D614G								
Gamma	P.1	K417T	**E484K**	N501Y	D614G	H655Y							
Omicron	BA.1	G339D	S371L	S373P	S375F	S477N	T478K	E484A	**Q493R**	G496S	Q498R	N501Y	
		Y505H	T547K	D614G	H655Y	N679K	P681H						
Omicron	BA.2.3.20	G339D	**S371F**	S373P	S375F	T376A	D405N	R408S	K417N	N440K	**K444R**	**N450D**	
		L452M	N460K	S477N	T478K	E484R	Q498R	N501Y	Y505H	D614G	H655Y	N679K	
		P681H											
Omicron	BA.2.77	G339D	**E340K**	K356T	**S371F**	S373P	S375F	T376A	D405N	R408S	K417N	N440K	
		L452R	S477N	T478K	E484A	Q498R	N501Y	Y505H	D614G	H655Y	N679K	P681H	
Omicron	BA.2.80	G339D	E340Q	R346T	K356T	**S371F**	S373P	S375F	T376A	D405N	R408S	K417N	
		N440K	S477N	T478K	E484A	**Q493R**	Q498R	N501Y	Y505H	Q564E	D614G	H655Y	
		N679K	P681H										
Omicron	BA.2	G339D	**S371F**	S373P	S375F	T376A	D405N	R408S	K417N	N440K	S477N	T478K	
		E484A	**Q493R**	Q498R	N501Y	Y505H	D614G	H655Y	N679K	P681H			
Omicron	BN.1	G339H	R346T	K356T	**S371F**	S373P	S375F	T376A	D405N	R408S	K417N	N440K	
		G446S	N460K	S477N	T478K	E484A	**F490S**	Q498R	N501Y	Y505H	D614G	H655Y	
		N679K	P681H										
Omicron	BQ.1	G339D	**S371F**	S373P	S375F	T376A	D405N	R408S	K417N	N440K	K444T	L452R	
		N460K	S477N	T478K	E484A	F486V	Q498R	N501Y	Y505H	D614G	H655Y	N679K	
		P681H											
Omicron	XBB	G339H	R346T	L368I	**S371F**	S373P	S375F	T376A	D405N	R408S	K417N	N440K	
		V445P	G446S	N460K	S477N	T478K	E484A	**F490S**	Q498R	N501Y	Y505H	D614G	
		H655Y	N679K	P681H									
Omicron	CH.1.1	G339H	R346T	**S371F**	S373P	S375F	T376A	D405N	R408S	K417N	N440K	K444T	
		G446S	L452R	N460K	S477N	T478K	E484A	F486S	Q498R	N501Y	Y505H	D614G	
		H655Y	N679K	P681H									
Omicron	HV.1.2	G339H	R346T	L368I	S371F	S373P	S375F	T376A	D405N	R408S	K417N	N440K	
		V445P	G446S	L452R	F456L	N460K	S477N	T478K	E484A	F486P	**F490S**	Q498R	
		N501Y	Y505H	**S514F**	D614G	H655Y	N679K	P681H					
Omicron	XBB.1.5	G339H	R346T	L368I	**S371F**	S373P	S375F	T376A	D405N	R408S	K417N	N440K	
		V445P	G446S	N460K	S477N	T478K	E484A	F486P	**F490S**	Q498R	N501Y	Y505H	
		D614G	H655Y	N679K	P681H								
Omicron	BA.2.87.1	G339D	**S371F**	S373P	S375F	T376A	D405N	R408S	K417T	N440K	K444N	V445G	
		L452M	N460K	S477N	N481K	E484A	Q498R	N501Y	Y505H	D614G	P621S	V642G	
		H655Y	N679R	P681H									

The table lists a selection of current variants of interest, variants under monitoring and de-escalated variants (as of July 26, 2024) based on the databases maintained by the European Centre for Disease Prevention and Control (ECDC, 2024), and the Lineage Reports by GISAID (Gangavarapu et al., 2023; Shruti et al., 2021). Among the Spike mutations of interest, mutations identified and studied in our selection experiments are color-coded based on the antibodies used for selection (Bamlanivimab, Sotrovimab, Cilgavimab, Bebtelovimab, S2K146, and S2H97). Mutations shown in **bold** are the exact amino acid mutations we identified in our selections. Otherwise, the selection had identified the same residue to be mutated, but not the same mutation (X = any amino acid substitution).

single Omicron subvariant BA.2.77 (NCBI, 2023; Wang et al., 2024). The identification of E340 as a critical site for neutralization by Sotrovimab, also found in an earlier in vitro study (Rockett et al., 2022), might help to predict the efficacy of Sotrovimab on virus variants that occur in the future.

Among the currently or previously circulating SARS-CoV-2 variants (Table 1), the Bamlanivimab resistance-associated mutations F490S or E484K/A are present in nearly all of them. Bebtelovimab and Cilgavimab resistance-conferring site V445 is mutated to G, H or P in the recent Omicron subvariants. The Sotrovimab resistance-conferring mutation E340K is contained within a single de-escalated variant. The K356 residue is mostly mutated to T in patients infected with the recent variants of interest, whereas our experiments selected for mutation K356M – however, both mutations would disrupt ionic interactions with Sotrovimab.

Among the studied mutations that confer resistance to S2K146 and S2H97, we observed that the mutations G485S + Q493R do not yet occur in the SARS-CoV-2 variants, though several variants emerged with

Q493R alone; similarly, among the mutations selected by S2H97, only S514F is identified in a single Omicron variant, while the others remain unobserved. This is likely because most of these mutations decrease Spike infectivity and ACE2 binding (Fig. 11C–D). Interestingly, the mutation selected by S2K146 – S371F – is present in nearly all the de-escalated variants of Omicron. Although S371F strongly reduces viral fitness, its infectivity is restored by other Spike mutations in these variants (such as N501Y, S477N, Q498R, and E484K) that enhance the RBD-ACE2 interaction (Cox et al., 2023; Dejnirattisai et al., 2022).

In summary, the mutations F490S, E484K, K444R, and N450D, frequently identified in our study, are also common in naturally occurring virus variants, making Bamlanivimab and Cilgavimab obsolete by now. In contrast, Sotrovimab and Bebtelovimab remained effective against most Omicron subvariants until the emergence of the current variants listed in Table 1. Hence, the mutations E340K, K356M and V445A are of particular concern if occurring in future virus variants. The mutation K462E conferring resistance to S2H97 is also of interest, as it enhances viral Spike infectivity. In general, in vitro selection of mutagenized virus pools provides a valuable approach to predict future antibody escape mutations.

3. Discussion

Our approach allowed the consistent identification of characteristic SARS-CoV-2-mutations within the Spike coding region that provide resistance to four different therapeutic antibodies, Bamlanivimab, Bebtelovimab, Cilgavimab and Sotrovimab, and two broadly-neutralizing antibodies, S2K146 and S2H97.

The combination of drug-induced mutagenesis with in vitro selection provides a technology platform for rapid and straightforward identification of mutations that allow the virus to escape from antibodies or other therapeutics. It may even be suitable for identifying escape-routes from the serum of a pre-immunized patient, by selecting viruses that escape the person's current composition of antibodies. The completeness of resistance, and the number of virus passages to achieve it may also provide an estimate of how rapidly such escape-mutants can arise in the real world, when COVID patients are undergoing therapy. Further improvements may include the continuous addition of NHC and/or additional mutagens while passaging the virus, to induce additional and complex mutations with more than one amino acid exchange. Similar approaches may also facilitate the pre-emptive identification of immune-escape variants of other viruses. NHC is effective on a number of RNA viruses, such as Influenza A/B viruses (Toots et al., 2019), Ebolavirus (Reynard et al., 2015), and Venezuelan Equine Encephalitis Virus (Urakova et al., 2018). Thus, NHC could be used as a mutagen for in vitro selection of such viruses, too.

Of note, all of the selected mutations encoded direct interaction sites between the Spike and the antibody, with the exception of S371F, which may provide resistance by disrupting the overall conformation of the Spike. In general, conformational mutations are more likely to destroy the interaction of Spike and ACE2, too, thus abolishing infectivity as observed in Fig. 11C–D. This is a major advantage of the selection from an infectious virus pool to predict resistant mutants. In contrast to mutagenesis and biochemical interaction analyses of mutant Spike-antibody (Cao et al., 2022; Francino-Urdaniz et al., 2021), or computational studies of changes in binding free energy upon mutations (Bai et al., 2021; Sharma et al., 2024), the selection of infectious viruses not only comprises antibody escape, but also maintains receptor binding and infectivity. The mutants selected in this way are therefore more likely to occur in the real world as epidemics proceed.

The mutations that confer resistance towards Bamlanivimab and Cilgavimab have emerged in major variants of interest of SARS-CoV-2 (Table 1). At the same time, the use of therapeutic antibodies has always been confined to a small fraction of patients with COVID, for reasons of cost and availability. Thus, the use of monoclonal antibodies is unlikely to shape the evolution of the virus in a patient population. This argues that Bamlanivimab and Cilgavimab bind to epitopes that are also frequent targets of naturally occurring antibodies. Hence, the natural immune response has conceivably selected virus variants that eliminate the same epitopes by mutation. This is in contrast to the mutation at E340, which confers resistance to Sotrovimab. This mutation is rare in natural virus mutants and does not belong to the spectrum of major Variants of Interest. Thus, Sotrovimab appears to target SARS-CoV-2 through an epitope that is less commonly used during the average immune response to the virus. Perhaps, this will render Sotrovimab more sustainable for treating infections with future variants of SARS-CoV-2. However, the emergence of mutations at residue K356 (Table 1) of the Spike protein could also affect Sotrovimab neutralization. Therefore, careful monitoring of emerging viruses for mutations at E340 and K356 is still advisable.

Similar to Sotrovimab, S2H97 targets a less used epitope of the Spike RBD, and the S2H97 resistance conferring mutations hardly occur naturally. While the mutation D428G reduced the Spike-ACE2 binding efficiency, the resistance-conferring mutation K462E enhanced ACE2 binding, and it therefore represents a mutation to monitor when implementing S2H97 therapeutically. S2K146, on the other hand, targets exactly the ACE2-binding residues on the Spike, and only a combination of two mutations, G485S + Q493R, could confer partial resistance while keeping the virus modestly infectious. Therefore, this antibody still holds promising therapeutic potential. Moreover, the strategy of targeting the receptor-binding surface of an envelope protein with antibodies may generally reduce the likelihood of resistance-conferring mutations.

In vitro mutagenesis requires careful handling to avoid the escape of mutant virus. It should be noted though that the prodrug of NHC, Molnupiravir, was a clinically approved drug in the UK (Syed, 2022), and it still holds Emergency Use Authorization by the FDA (FDA, 2023b; Mia et al., 2024). Thus, precautions should also be applied when treating patients with it, to avoid the formation and spread of gain-of-function variants, as we have outlined in more detail previously (Zibat et al., 2023).

The importance of understanding SARS-CoV-2 evolution has led to a number of other studies with different approaches to identify Spike mutations that interfere with antibody binding. One study describes a machine learning approach investigating a large number of SARS-CoV-2 RBD sequences with combined mutations, to identify mutations that preserve ACE2 binding but disrupt the interaction with antibodies (Taft et al., 2022). More recently, a library of combined mutations was displayed on pseudoviruses and tested for antibody neutralization (Dadonaite et al., 2023). Similarly, an inverted infection assay using ACE2-harboring viruses was used to find mutations from a library of mutant Spike-expressing cells in the presence of neutralizing antibody (Alcantara et al., 2023). While such mutation scanning methods sample a large number of Spike mutations, they only partially recapitulate the evolution of fully infectious, antibody-evading SARS-CoV-2 mutants and thus require the construction of recombinant viruses to confirm the impact of individual mutations.

In our study, the selection of escape-mutations from an Omicron B.1.1.529 strain took more rounds compared to the Wuhan-like virus (Fig. 5A, Fig. S7 A, Fig. S15). One reason for this may be that Omicron, in general, is less immunogenic (Mannar et al., 2022). Moreover, the Omicron Spike binds ACE2 with up to 9-fold increased affinity compared to Wuhan (Yin et al., 2022), perhaps shifting the equilibrium from antibody-bound to receptor-bound Spike. Accordingly, a higher concentration of Cilgavimab was needed to neutralize Omicron. The Omicron Spike RBD is conformationally more dynamic in its apo-form (Yin et al., 2022), which may decrease the opportunities for antibodies to bind it. Thus, the window of opportunity between the initial Omicron pools and the escape mutants seems smaller than in the case of Wuhan-like strains.

Taken together, the in vitro selection of NHC-derived virus pools enables the identification of immune-escape SARS-CoV-2 mutants. We

propose that this approach will be useable to generate a catalogue of such mutants for future therapeutic antibodies and antiviral compounds, before such escape-mutations even occur in patients.

3.1. Limitations of the study

One of the limitations of using this platform for generating virus mutants consists in biases caused by NHC. When NHC is incorporated into nascent viral RNA, tautomeric interconversions allow it to base pair with guanine as well as adenine in the subsequent replication steps. Thus, NHC mutagenesis is largely limited to transitions rather than transversions (Bessi et al., 2024; Janion and Glickman, 1980; Zibat et al., 2023) and does not generate a comprehensive collection of mutations. Additionally, during passaging in the presence of antibodies, it is possible to reach bottlenecks during the selection process. In this scenario, an insufficient number of mutants would not fill the sequence space of potential variants.

Another consideration is that our study was conducted in vitro, which differs from an infection of patients by the immune and inflammatory response. In an individual infected with SARS-CoV-2, the development of resistance-conferring mutations upon treatment with a therapeutic antibody may be affected by multiple endogenous antibodies. Further, T-cell epitopes of the Spike may influence the selection of mutations in vivo.

Hence, the system described here reflects only partially how viruses can accumulate mutations in patients. Nonetheless, it does reveal at least a subset of virus mutations that can counteract the efficacy of therapeutic antibodies.

4. Materials and methods

4.1. Cell culture

Vero E6 cells (Vero C1008) were used as host cells for SARS-CoV-2 and VSV-pseudotype infection; BHKG43 and HEK293T cells for VSV-pseudotype preparation; and HeLa cells for Spike overexpression and immunofluorescence staining. The following table describes sources and media. Cells were incubated in a humidified atmosphere with 5% CO_2 at 37 °C.

Cell Line	Source	Basal Medium	Supplements
Vero E6	German Primate Centre (DPZ), Göttingen, Germany	Dulbecco's modified Eagle's medium (DMEM) with GlutaMAX™, Gibco	10% fetal bovine serum (FBS; Merck), 200 μM L-Glutamine, 50 U/mL penicillin (Gibco), 50 μg/mL streptomycin (Gibco), 2 μg/mL tetracycline (Sigma), 10 μg/mL ciprofloxacin (Bayer)
HEK293T	German Collection of Microorganisms and Cell Cultures (DSMZ), Braunschweig, Germany	Dulbecco's modified Eagle's medium (DMEM)	
HeLa	ATCC	Dulbecco's modified Eagle's medium (DMEM)	
BHK 21 (G43)	DPZ	Eagle's minimum essential medium (EMEM)	10% fetal bovine serum (FBS; Merck), 200 μM L-Glutamine, 50 U/mL penicillin (Gibco), 50 μg/mL streptomycin (Gibco), 50 μg/mL Hygromycin B (Invitrogen), 100 μg/ml Zeocin (Invitrogen)

4.2. Treatments and SARS-CoV-2 infection

A Wuhan-like SARS-CoV-2 strain (mutations with respect to reference NC_045512.2: Nsp2: T85I, RdRp: P323L, S: D614G, ORF3a: Q57H) was isolated in Göttingen in March 2020 (Stegmann et al., 2021) and is referred to as 'Wuhan'.

2.5×10^5 Vero E6 cells were seeded in t25 flasks with medium containing 10% FBS. After 24 h, the medium was replaced to contain 2% FBS and 400 nM β-D-N^4-hydroxycytidine (NHC/EIDD-1931, Cayman Chemical 9002958), followed by an incubation of 1 h at 37 °C before infection.

The cells were then infected with SARS-CoV-2 (Wuhan-like) at MOI 0.08, corresponding to 2×10^4 focus forming units (FFU), and incubated for 48 h at 37 °C to obtain a pool of SARS-CoV-2 mutants in the cell supernatant. An amount corresponding to ~2×10^{10} viral RNA copies from this virus pool was used for re-infecting 2.5×10^5 Vero E6 cells in the presence of 400 nM NHC, to complete two rounds of mutagenesis.

For selecting antibody-resistant mutants, the virus pools were incubated in increasing concentrations of antibodies (described in Figs. 1A and 9A) for 1 h at 37 °C (in three or four individual passages). The following antibodies were used:

Antibody	Source	Selection of virus strains
Bamlanivimab	Eli Lilly and Company, GTIN: 00300027910017	Wuhan
Sotrovimab	Proteogenix, PX-TA1637 or GSK Sotrovimab (Xevudy) Lot GX2C	Wuhan, B.1.1.529
Cilgavimab	Proteogenix, PX-TA1033	Wuhan, B.1.1.529
Bebtelovimab	Proteogenix, PX-TA1750	B.1.1.529
S2K146	Proteogenix, PTXCOV-A582	Wuhan
S2H97	Proteogenix, PTXCOV-A580	Wuhan

Subsequently, Vero E6 cells were incubated with the antibody-virus mix for 48 h at 37 °C. In each passage, the amount of virus added to cells was adjusted after quantification by qPCR.

For neutralization assays to determine the degrees of resistance, different virus pools were pre-incubated with different antibody dilutions (37 °C, 1 h) and used to infect Vero E6 cell monolayers for 48 h, followed by immunofluorescence analysis as described below.

For mutagenesis and selection experiments with the Omicron strain (B.1.1.529; European Virus Archive Global Ref-SKU: 009V-04437, obtained from the Robert Koch Institute, Berlin, Germany), 100–200 nM NHC was used for mutagenesis. Here, lower amounts of NHC were used as compared to the Wuhan strain because B.1.1.529 showed higher sensitivity to NHC (Fig. S16), in agreement with a previous study (Li et al., 2022). The virus pools were passaged six times with increasing concentrations of antibodies (cf. table above, Fig. 5A).

4.3. Quantitative RT-PCR for virus quantification

The virus samples were first inactivated in a 1:1 ratio of media and the GTC Lysis Binding Buffer from the MagNA Pure LC Total Nucleic Acid Isolation Kit (Roche). Viral RNA was isolated through Trizol LS, chloroform extraction and isopropanol precipitation. The subsequent RNA pellet was washed with 75% ethanol, dried and resuspended in nuclease-free water. Both Wuhan and B.1.1.529 virus RNA were quantified by RT-qPCR with a TaqMan probe, using the following primers to

amplify a conserved region of the SARS-CoV-2 envelope protein gene (nucleotides 26,141–26,253) (Corman et al., 2020).

Primer	5' – Sequence – 3'	Modification
F (forward)	ACAGGTACGTTAATAGTTAATAGCGT	–
R (reverse)	ATATTGCAGCAGTACGCACACA	–
P (probe)	ACACTAGCCATCCTTACTGCGCTTCG	5' 6-carboxyfluorescein (FAM), 3' Blackberry Quencher (BBQ)

4.4. Deep sequencing

Novogene UK performed library preparations for the viral RNA of Wuhan samples selected with Bamlanivimab/Sotrovimab/Cilgavimab. Library preparations for the remaining Wuhan and B.1.1.529 selected viral RNA were performed using the QIAseq DIRECT SARS-CoV-2 Kit A (#333891). Novogene UK performed sequencing for all the samples. The RNA samples were reverse transcribed into cDNA and amplified by multiplex PCR amplification capture (MultipSeq®). After library quality check, the libraries were sequenced on Illumina NovaSeq 6000 (PE 150 bp; 2G raw data per sample). Raw reads were deposited at NCBI SRA, BioProject ID: PRJNA1143956.

4.5. Sequencing data processing and variant calling

The first analysis of Wuhan strain antibody selection (Passages 0 and 3) was performed as follows: FASTQ files were assessed for quality using FastQC v0.11.9 (Andrews, 2010). The adapter sequences were trimmed using trim_galore version 0.6.7, (https://www.bioinformatics.babraham.ac.uk/projects/trim_galore/), and contaminating host cell reads were removed by kraken2 version 2.1.2 (Wood and Salzberg, 2014). Finally, the processed reads were mapped to the SARS-CoV-2 reference genome NC 045512.2 with BWA-mem version 0.7.17-r1188 (Li and Durbin, 2009). Samtools version 1.15 (Li et al., 2009) was used to sort and index the subsequent BAM files. Variant calling was performed using FreeBayes v1.3.6 (Garrison and Marth, 2012), with a minimum alternate allele frequency threshold of 0.05. This generated VCF files which were then split using the vcfbreakmulti function from the vcflib version 1.0.3 (Garrison et al., 2022). Finally the called variants were annotated using SnpEff version 4.5covid19 (Cingolani et al., 2012). For all other Wuhan and B.1.1.529 sequencing data, we followed the same processing steps except for low-quality sequence trimming, which was performed using CutAdapt version 2.3, (Martin, 2011); mapping to reference genome, which was done using BowTie2 version 2.3.4.1, (Langmead and Salzberg, 2012); variant calling, which was performed with a minimum alternate allele frequency 0.01; and variant annotation, which was done using SnpEff version 4.37.

The above processing steps allowed us to identify mutations including the pre-existing ones from the initial pool of B.1.1.529. Subsequently, for the B.1.1.529 selection study, we filtered out the mutations that were (1) common to antibody-selected virus pools and the original Omicron B.1.1.529 strain, and/or (2) present in the virus pools passaged without antibody with alteration frequency greater than 0.04. This allowed us to shortlist the possible resistance-conferring mutations as plotted in Fig. 6.

4.6. Preparation of single spike mutation pseudotypes for neutralization assays

A vesicular stomatitis virus (VSV) system was employed for the preparation of pseudotypes, i.e. viruses displaying envelope proteins that do not belong to their species. Recombinant VSV particles (VSV*ΔG-F-Luc-G) that contain genes encoding Green Fluorescent Protein (GFP) and Firefly Luciferase (F-Luc) in place of the VSV-G glycoprotein gene in their genome (Sidarovich et al., 2022), were kindly provided by Gert Zimmer (Berger Rentsch and Zimmer, 2011; Zimmer et al., 2014). In order to produce VSV*ΔG-F-Luc-G virus stocks, the virus was propagated for 24 h at 37 °C in BHK-21 (G43) cells (kindly provided by Stefan Pöhlmann, DPZ, Göttingen), which were induced to overexpress VSV-G glycoprotein using 10 nM Mifepristone (Sigma) (Berger Rentsch and Zimmer, 2011). Virus aliquots were stored in −70 °C.

In order to produce VSV*ΔG-F-Luc-SARS-CoV-2-S pseudotypes, 1.5 × 10^6 HEK293T cells, seeded in 100-mm cell culture plates, were transfected with plasmids (cf. the table below) to express wildtype or mutant SARS-CoV-2 Spike, using Lipofectamine 3000 (Life technologies) for 24 h at 37 °C. Afterwards, the transfection media was replaced by a VSV*ΔG-F-Luc-G virus stock at MOI 2 in media containing 2% FBS, for 1–2 h at 37 °C. The virus-containing media was then replaced by fresh media containing 2% FBS and 500 ng/mL anti-VSV-G antibody (Kerafast), to neutralize any non-pseudotyped VSV*ΔG-F-Luc-G that might have been carried over from the initial stock. The cells were incubated for another 18 h at 37 °C, and the supernatants containing VSV-Spike-pseudotypes were harvested.

To test their susceptibility to antibodies or hACE2 (10108-H02H, SinoBiologicals), wildtype or mutant Spike pseudotypes were incubated with antibody dilutions in 2% FBS media for 1–2 h at 37 °C. Then, the pseudotype-antibody (or hACE2) mixture was added on top of Vero E6 cell monolayer overnight at 37 °C. Infected cells were then identified by detecting the green fluorescent signal derived from the GFP encoded by the VSV-dG*S genome, using a Celigo Image cytometer (Nexcelom). Neutralization efficacies were calculated by dividing the number of infected cells in a well by the number of infected cells in a control well without antibody or hACE2.

4.7. Generation of spike expression plasmids by site-directed mutagenesis

The Spike expression plasmid was originally purchased from Sino-Biologicals (Cat# VG40589-UT, VG40835-UT). The Spike gene was then truncated by a 19-amino acid carboxyterminal deletion (Δ19-aa), by site directed mutagenesis using QuikChange XL kit (Agilent), to improve pseudotype infectivity (Chen et al., 2021a; Johnson et al., 2020). The same mutagenesis protocol was then used to introduce individual Spike mutations to be tested for antibody resistance. The mutations introduced were confirmed by Sanger sequencing (Eurofins). The following table indicates the sequences of oligonucleotide used for each mutagenesis.

Spike Expression Plasmid	Spike Modifications and primer pair
Wuhan Spike pCMV3-SARS-CoV-2-S-Δ19	Wuhan Spike pCMV3-SARS-CoV-2-S Sino Biological (Cat# VG40589-UT) + **Δ19-aa**: 5'-ctgtggctcctgttgtaagtaggatgaggtaccctctgaacctgtgctg-3' 5'-cagcacaggttcagagggtacctcatcctacttacaacaggagccacag-3'
Wuhan Spike pCMV3-SARS-CoV-2-S-Δ19-E340K	Wuhan Spike pCMV3-SARS-CoV-2-S-Δ19 + **E340K**: 5'- ccaacctgtgtccatttggaaaggtgttcaatgcc-3' 5'-ggcattgaacacctttccaaatggacacaggttgg-3'
Wuhan Spike pCMV3-SARS-CoV-2-S-Δ19-E484K	Wuhan Spike pCMV3-SARS-CoV-2-S-Δ19 + **E484K**: 5'-caccatgtaatggagtgaagggcttcaactgttac-3' 5'-gtaacagttgaagcccttcactccattacatggtg-3'
Wuhan Spike pCMV3-SARS-CoV-2-S-Δ19-F490S	Wuhan Spike pCMV3-SARS-CoV-2-S-Δ19 + **F490S**: 5'-ggagggcttcaactgttacagtccactccaatcctatgg-3' 5'-gccataggattggagtggactgtaacagttgaagccctcc-3'

(continued on next page)

(*continued*)

Spike Expression Plasmid	Spike Modifications and primer pair
Wuhan Spike pCMV3-SARS-CoV-2-S-Δ19-K444E	Wuhan Spike pCMV3-SARS-CoV-2-S-Δ19 + **K444E**: 5′- acaacctggacagcgaggtgggaggcaac-3′ 5′- gttgcctcccacctcgctgtccaggttgt-3′
Wuhan Spike pCMV3-SARS-CoV-2-S-Δ19-K444R	Wuhan Spike pCMV3-SARS-CoV-2-S-Δ19 + **K444R**: 5′- acaacctggacagcagggtgggaggcaac-3′ 5′- gttgcctcccaccctgctgtccaggttgt-3′
Wuhan Spike pCMV3-SARS-CoV-2-S-Δ19-N450D	Wuhan Spike pCMV3-SARS-CoV-2-S-Δ19 + **N450D**: 5′- ggtgggaggcaactacgactacctctacagact-3′ 5′- agtctgtagaggtagtcgtagttgcctcccacc-3′
Wuhan Spike pCMV3-SARS-CoV-2-S-Δ19-S494P	Wuhan Spike pCMV3-SARS-CoV-2-S-Δ19 + **S494P**: 5′- actttccactccaaccctatggcttccaaccaacc-3′ 5′- ggttggttggaagccatagggttggagtggaaag-3′
B.1.1.529 Spike pCMV3-SARS-CoV-2-S-Δ19	B.1.1.529 Spike pCMV3-SARS-CoV-2-S Sino Biological (Cat# VG40835-UT) + **Δ19-aa**: 5′-ctgtggctcctgttgtaagtaggatgaggtaccctctgaacctgtgctg-3′ 5′-cagcacaggttcagagggtacctcatcctacttacaacaggagccacag-3′
B.1.1.529 Spike pCMV3-SARS-CoV-2-S-Δ19-E340K	B.1.1.529 Spike pCMV3-SARS-CoV-2-S-Δ19 + **E340K**: 5′- acctgtgtccatttgacaaggtgttcaatgccacc-3′ 5′- acctgtgtccatttgacaaggtgttcaatgccacc-3′
B.1.1.529 Spike pCMV3-SARS-CoV-2-S-Δ19-K356M	B.1.1.529 Spike pCMV3-SARS-CoV-2-S-Δ19 + **K356M**: 5′- ctatgcctggaacaggatgaggattagcaactgtg-3′ 5′- cacagttgctaatcctcatcctgttccaggcatag-3′
B.1.1.529 Spike pCMV3-SARS-CoV-2-S-Δ19-K444R	B.1.1.529 Spike pCMV3-SARS-CoV-2-S-Δ19 + **K444R**: 5′- acaagctggacagcagggtgagcggcaac-3′ 5′- gttgccgctcaccctgctgtccagcttgt-3′
B.1.1.529 Spike pCMV3-SARS-CoV-2-S-Δ19-N450D	B.1.1.529 Spike pCMV3-SARS-CoV-2-S-Δ19 + **N450D**: 5′- ggtgagcggcaactacgactacctctacagact-3′ 5′- agtctgtagaggtagtcgtagttgccgctcacc-3′
B.1.1.529 Spike pCMV3-SARS-CoV-2-S-Δ19-V445A	B.1.1.529 Spike pCMV3-SARS-CoV-2-S-Δ19 + **V445A**: 5′- caagctggacagcaaggcgagcggcaactacaac-3′ 5′- gttgtagttgccgctcgccttgctgtccagcttg-3′
Wuhan Spike pCMV3-SARS-CoV-2-S-Δ19-S371F	Wuhan Spike pCMV3-SARS-CoV-2-S-Δ19 + **S371F**: 5′-tgactactctgtgctctacaactttgcctccttcag-3′ 5′-ctgaaggaggcaaagttgtagagcacagagtagtca-3′
Wuhan Spike pCMV3-SARS-CoV-2-S-Δ19-D428G	Wuhan Spike pCMV3-SARS-CoV-2-S-Δ19 + **D428G**: 5′-ctacaaactgcctgatggcttcacaggctgtgtga-3′ 5′-tcacacagcctgtgaagccatcaggcagtttgtag-3′
Wuhan Spike pCMV3-SARS-CoV-2-S-Δ19-K462E	Wuhan Spike pCMV3-SARS-CoV-2-S-Δ19 + **K462E**: 5′- gttcaggaagagcaacctggagccatttgagagggacatca-3′ 5′- tgatgtccctctcaaatggctccaggttgctcttcctgaac-3′
Wuhan Spike pCMV3-SARS-CoV-2-S-Δ19-G485S	Wuhan Spike pCMV3-SARS-CoV-2-S-Δ19 + **G485S**: 5′-ccatgtaatggagtggagagcttcaactgttactttc-3′ 5′-gaaagtaacagttgaagctctccactccattacatgg-3′
Wuhan Spike pCMV3-SARS-CoV-2-S-Δ19-Q493R	Wuhan Spike pCMV3-SARS-CoV-2-S-Δ19 + **Q493R**: 5′-ttcaactgttactttccactcagatcctatggcttccaaccaac-3′ 5′-gttggttggaagccataggatctgagtggaaagtaacagttgaa-3′
Wuhan Spike pCMV3-SARS-CoV-2-S-Δ19-S514F	Wuhan Spike pCMV3-SARS-CoV-2-S-Δ19 + **S514F**: 5′-gggtggtggtgctgttctttgaactgctcca-3′ 5′-tggagcagttcaaagaacagcaccaccaccc-3′
Wuhan Spike pCMV3-SARS-CoV-2-S-Δ19-D574N	Wuhan Spike pCMV3-SARS-CoV-2-S-Δ19 + **D574N**: 5′-cattgctgacaccacaaatgctgtgagggaccc-3′ 5′-gggtccctcacagcatttgtggtgtcagcaatg-3′

4.8. Immunofluorescence analysis

For immunofluorescence analyses of SARS-CoV-2 infected cells, the cells were first fixed with 4% paraformaldehyde (Sigma) in PBS for 1 h at room temperature (RT). The fixed cells were then permeabilized with 0.5% Triton X-100 (Sigma-Aldrich) in PBS at RT for 20 min and blocked with 10% FCS (Anprotec) in PBS at RT for 30 min. The primary antibody was anti-Nucleoprotein antibody (Hölzel), incubated in a 1:8000 dilution in PBS/10%FCS at 4 °C overnight, and the secondary antibody staining was done using donkey anti-rabbit-IgG antibodies coupled to Alexa Fluor 488 (Thermofisher; 1:500 dilution) alongside 4′,6-diamidino-2-phenylindole (DAPI) staining (Sigma; 1:3000 dilution) at RT for 1–2 h. Fixation, permeabilization and antibody staining steps were each followed by two to three PBS washes of 5 min.

Imaging of fixed and stained plates was performed using a Celigo Image cytometer (Nexcelom). Infected cells were counted using the software ImageJ (1.53k/Java-1.8.0_172) based on the SARS-CoV-2 Nucleoprotein-derived signal. The percentage of infected cells was calculated by dividing the number of infected cells with the number of DAPI stained nuclei and multiplying by 100.

For immunostaining of wildtype or mutant Spike proteins upon overexpression in HeLa cells, Bamlanivimab/Sotrovimab/Cilgavimab/Bebtelovimab/S2K146/S2H97 were used as primary antibodies in the following concentrations:

Wildtype/Mutant Spike of	Primary Antibody	Concentration (μg/mL)
Wuhan	Bamlanivimab	5
	Sotrovimab	5
	Cilgavimab	5
B.1.1.529	Bebtelovimab	5
	Sotrovimab	5
	Cilgavimab	30
Wuhan	S2K146	0.1
	S2H97	2

For secondary staining, anti-human IgG AF488 (Jackson ImmunoResearch 109-545-003 or Invitrogen A-10631) was used at concentration 5 μg/mL. Primary staining was performed either at 4 °C overnight or for 1–2 h at RT. In parallel, an anti-Spike mouse antibody that binds to the S2 region of the Spike (Gene Tex, Cat #GTX632604, 1:2000 dilution) was used to visualize the Spike expression irrespective of the mutations, using a donkey anti-mouse IgG secondary antibody coupled to AF546 (Invitrogen, 1:500 dilution).

4.9. Structure modeling of the spike-antibody complexes

The Spike mutations selected by Bamlanivimab/Sotrovimab/Cilgavimab were mapped on the Spike structure from PDB 7kj4 (Xiao et al., 2021) and visualized on PyMOL version 4.6 (Schrodinger, 2015). The PDB structure 7l3n (Jones et al., 2021) shows Wuhan Spike protein bound to Bamlanivimab. This structure was used to examine the Spike residues mutated upon Bamlanivimab selection. Similarly, Wuhan Spike mutations selected by other antibodies were investigated based on the PDB structures 6wps (Pinto et al., 2020) and 7l7e (Dong et al., 2021) for Sotrovimab and Cilgavimab, respectively.

The PDB structure 7wpc (Yin et al., 2022) of the B.1.1.529 Spike bound to ACE2 was used to depict antibody-selected mutations on this Spike variant. Interactions between Sotrovimab and the B.1.1.529 RBD were visualized on the PDB structure 7yad (Zhao et al., 2022), displaying the two proteins in a complex. Interactions between Bebtelovimab or Cilgavimab and the B.1.1.529 Spike were predicted by superimposing the B.1.1.529 Spike structure from PDB 7wpc (Yin et al., 2022) onto the PDB structure 7mmo displaying the complex of Bebtelovimab and the Wuhan Spike (Westendorf et al., 2022), or onto the PDB structure 7l7e that shows the complex of Cilgavimab with the Wuhan Spike (Dong et al., 2021).

Mutations selected by S2K146 and S2H97 were mapped on the PDB structures 7tas (Park et al., 2022) and 7m7w (Starr et al., 2021a), respectively; the same structures were also used to visualize S2K146-RBD and S2H97-RBD interactions.

Data availability

NGS data associated to this project is available at NCBI SRA with the BioProject ID: PRJNA1143956.

CRediT authorship contribution statement

Priya Kumar: Writing – review & editing, Visualization, Validation, Methodology, Investigation, Formal analysis, Data curation, Conceptualization. **Xiaoxiao Zhang:** Visualization, Validation, Methodology, Formal analysis, Data curation. **Rahul Shaha:** Visualization, Methodology, Formal analysis, Data curation. **Maik Kschischo:** Supervision, Project administration, Funding acquisition. **Matthias Dobbelstein:** Writing – review & editing, Writing – original draft, Supervision, Project administration, Investigation, Funding acquisition, Conceptualization.

Declaration of competing interest

The other authors declare no conflict of interest.

Data availability

All data are displayed in the figures and tables, including supplemental figures and tables.

Acknowledgements

PK was a member of the IMPRS/MSc program Molecular Biology and the Göttingen Graduate School GGNB during this work.

This work was funded by the VolkswagenStiftung (AZ 9A827 and AZ 9B785) to MD, by the COVID-19 Forschungsnetzwerk Niedersachsen (COFONI) to MD, and the German Federal Ministry of Education and Research (BMBF) to MK (13FH005KI2). MD is a fellow at the Max Planck Institute for Multidisciplinary Sciences MPI-NAT. XZ was supported by a grant of the Ministry of sciences and health of Rhineland-Palatinate, Germany (COVID-AI).

We sincerely thank Dr. Gert Zimmer and Dr. Stefan Pöhlmann for providing us with the material and guidance for establishing the VSV-pseudotype system in our lab. We also extend our thanks to Sebastian Schimkowiak for his assistance with RNA isolations and plasmid preparations.

Appendix A. Supplementary data

Supplementary data to this article can be found online at https://doi.org/10.1016/j.antiviral.2024.106006.

References

Abenavoli, L., 2024. The COVID-19 pandemic is over, but the virus still lingers. Diseases 12, 57. https://doi.org/10.3390/diseases12030057.

Alcantara, M.C., Higuchi, Y., Kirita, Y., Matoba, S., Hoshino, A., 2023. Deep mutational scanning to predict escape from bebtelovimab in SARS-CoV-2 omicron subvariants. Vaccines 11. https://doi.org/10.3390/vaccines11030711.

Andrews, S., 2010. FastQC - a quality control tool for high throughput sequencing data. Babraham Bioinformatics. http://www.bioinformatics.babraham.ac.uk/projects/fastqc/.

Bai, C., Wang, J., Chen, G., Zhang, H., An, K., Xu, P., Du, Y., Ye, R.D., Saha, A., Zhang, A., Warshel, A., 2021. Predicting mutational effects on receptor binding of the spike protein of SARS-CoV-2 variants. J. Am. Chem. Soc. 143, 17646–17654. https://doi.org/10.1021/jacs.1c07965.

Berger Rentsch, M., Zimmer, G., 2011. A vesicular stomatitis virus replicon-based bioassay for the rapid and sensitive determination of multi-species type I interferon. PLoS One 6, e25858. https://doi.org/10.1371/journal.pone.0025858.

Bessi, I., Stiller, C., Schroeder, T., Schäd, B., Grüne, M., Dietzsch, J., Höbartner, C., 2024. The tautomeric state of N4-hydroxycytidine within base-paired RNA. ACS Cent. Sci. 10, 1084–1093. https://doi.org/10.1021/acscentsci.4c00146.

Birnie, E., Biemond, J.J., Appelman, B., de Bree, G.J., Jonges, M., Welkers, M.R.A., Wiersinga, W.J., 2022. Development of resistance-associated mutations after Sotrovimab administration in high-risk individuals infected with the SARS-CoV-2 omicron variant. JAMA 328, 1104–1107. https://doi.org/10.1001/jama.2022.13854.

Brady, T., Zhang, T., Tuffy, K.M., Haskins, N., Du, Q., Lin, J., Kaplan, G., Novick, S., Roe, T.L., Ren, K., 2022. Qualification of a biolayer interferometry assay to support AZD7442 resistance monitoring. Microbiol. Spectr. 10, e01034, 01022.

Cameroni, E., Bowen, J.E., Rosen, L.E., Saliba, C., Zepeda, S.K., Culap, K., Pinto, D., VanBlargan, L.A., De Marco, A., di Iulio, J., Zatta, F., Kaiser, H., Noack, J., Farhat, N., Czudnochowski, N., Havenar-Daughton, C., Sprouse, K.R., Dillen, J.R., Powell, A.E., Chen, A., Maher, C., Yin, L., Sun, D., Soriaga, L., Bassi, J., Silacci-Fregni, C., Gustafsson, C., Franko, N.M., Logue, J., Iqbal, N.T., Mazzitelli, I., Geffner, J., Grifantini, R., Chu, H., Gori, A., Riva, A., Giannini, O., Ceschi, A., Ferrari, P., Cippà, P.E., et al., 2022. Broadly neutralizing antibodies overcome SARS-CoV-2 Omicron antigenic shift. Nature 602, 664–670. https://doi.org/10.1038/s41586-021-04386-2.

Cao, Y., Jian, F., Wang, J., Yu, Y., Song, W., Yisimayi, A., Wang, J., An, R., Chen, X., Zhang, N., Wang, Y., Wang, P., Zhao, L., Sun, H., Yu, L., Yang, S., Niu, X., Xiao, T., Gu, Q., Shao, F., Hao, X., Xu, Y., Jin, R., Shen, Z., Wang, Y., Xie, X.S., 2023. Imprinted SARS-CoV-2 humoral immunity induces convergent Omicron RBD evolution. Nature 614, 521–529. https://doi.org/10.1038/s41586-022-05644-7.

Cao, Y., Wang, J., Jian, F., Xiao, T., Song, W., Yisimayi, A., Huang, W., Li, Q., Wang, P., An, R., Wang, J., Wang, Y., Niu, X., Yang, S., Liang, H., Sun, H., Li, T., Yu, Y., Cui, Q., Liu, S., Yang, X., Du, S., Zhang, Z., Hao, X., Shao, F., Jin, R., Wang, X., Xiao, J., Wang, Y., Xie, X.S., 2022. Omicron escapes the majority of existing SARS-CoV-2 neutralizing antibodies. Nature 602, 657–663. https://doi.org/10.1038/s41586-021-04385-3.

Carabelli, A.M., Peacock, T.P., Thorne, L.G., Harvey, W.T., Hughes, J., de Silva, T.I., Peacock, S.J., Barclay, W.S., de Silva, T.I., Towers, G.J., Robertson, D.L., Consortium, C.-G.U., 2023. SARS-CoV-2 variant biology: immune escape, transmission and fitness. Nat. Rev. Microbiol. 21, 162–177. https://doi.org/10.1038/s41579-022-00841-7.

Cathcart, A.L., Havenar-Daughton, C., Lempp, F.A., Ma, D., Schmid, M.A., Agostini, M.L., Guarino, B., iulio, J.D., Rosen, L.E., Tucker, H., Dillen, J., Subramanian, S., Sloan, B., Bianchi, S., Pinto, D., Saliba, C., Culap, K., Wojcechowskyj, J.A., Noack, J., Zhou, J., Kaiser, H., Lee, S., Farhat, N., Chase, A., Montiel-Ruiz, M., Exequiel Dellota, J., Park, A., Spreafico, R., Sahakyan, A., Lauron, E.J., Czudnochowski, N., Cameroni, E., Ledoux, S., Kawaoka, Y., Werts, A., Colas, C., Soriaga, L., Telenti, A., Purcell, L.A., Hwang, S., et al., 2022. The dual function monoclonal antibodies VIR-7831 and VIR-7832 demonstrate potent in vitro and in vivo activity against SARS-CoV-2. bioRxiv, 434607. https://doi.org/10.1101/2021.03.09.434607, 2021.2003.2009.

Chen, H.Y., Huang, C., Tian, L., Huang, X., Zhang, C., Llewellyn, G.N., Rogers, G.L., Andresen, K., O'Gorman, M.R.G., Chen, Y.W., Cannon, P.M., 2021a. Cytoplasmic tail truncation of SARS-CoV-2 spike protein enhances titer of pseudotyped vectors but masks the effect of the D614G mutation. J. Virol. 95, e0096621 https://doi.org/10.1128/JVI.00966-21.

Chen, P., Datta, G., Grace Li, Y., Chien, J., Price, K., Chigutsa, E., Brown-Augsburger, P., Poorbaugh, J., Fill, J., Benschop, R.J., Rouphael, N., Kay, A., Mulligan, M.J., Saxena, A., Fischer, W.A., Dougan, M., Klekotka, P., Nirula, A., Benson, C., 2021b. First-in-Human study of bamlanivimab in a randomized trial of hospitalized patients with COVID-19. Clin. Pharmacol. Therapeut. 110, 1467–1477. https://doi.org/10.1002/cpt.2405.

Chen, R.E., Winkler, E.S., Case, J.B., Aziati, I.D., Bricker, T.L., Joshi, A., Darling, T.L., Ying, B., Errico, J.M., Shrihari, S., VanBlargan, L.A., Xie, X., Gilchuk, P., Zost, S.J., Droit, L., Liu, Z., Stumpf, S., Wang, D., Handley, S.A., Stine, W.B., Shi, P.-Y., Davis-Gardner, M.E., Suthar, M.S., Knight, M.G., Andino, R., Chiu, C.Y., Ellebedy, A.H., Fremont, D.H., Whelan, S.P.J., Crowe, J.E., Purcell, L., Corti, D., Boon, A.C.M., Diamond, M.S., 2021c. In vivo monoclonal antibody efficacy against SARS-CoV-2 variant strains. Nature 596, 103–108. https://doi.org/10.1038/s41586-021-03720-y.

Choudhary, M.C., Chew, K.W., Deo, R., Flynn, J.P., Regan, J., Crain, C.R., Moser, C., Hughes, M.D., Ritz, J., Ribeiro, R.M., Ke, R., Dragavon, J.A., Javan, A.C., Nirula, A., Klekotka, P., Greninger, A.L., Fletcher, C.V., Daar, E.S., Wohl, D.A., Eron, J.J., Currier, J.S., Parikh, U.M., Sieg, S.F., Perelson, A.S., Coombs, R.W., Smith, D.M., Li, J.Z., Smith, D., Javan, A.C., Giganti, M., Hosey, L., Roa, J., Patel, N., Colsh, K., Rwakazina, I., Beck, J., Sieg, S., Fischer, W., Evering, T., Ignacio, R.B., et al., 2022. Emergence of SARS-CoV-2 escape mutations during Bamlanivimab therapy in a phase II randomized clinical trial. Nature Microbiology 7, 1906–1917. https://doi.org/10.1038/s41564-022-01254-1.

Cingolani, P., Platts, A., Wang le, L., Coon, M., Nguyen, T., Wang, L., Land, S.J., Lu, X., Ruden, D.M., 2012. A program for annotating and predicting the effects of single nucleotide polymorphisms. Fly 6, 80–92. https://doi.org/10.4161/fly.19695.

Cohen, M.S., Nirula, A., Mulligan, M.J., Novak, R.M., Marovich, M., Yen, C., Stemer, A., Mayer, S.M., Wohl, D., Brengle, B., Montague, B.T., Frank, I., McCulloh, R.J., Fichtenbaum, C.J., Lipson, B., Gabra, N., Ramirez, J.A., Thai, C., Chege, W., Gomez Lorenzo, M.M., Sista, N., Farrior, J., Clement, M.E., Brown, E.R., Custer, K.L., Van Naarden, J., Adams, A.C., Schade, A.E., Dabora, M.C., Knorr, J., Price, K.L., Sabo, J., Tuttle, J.L., Klekotka, P., Shen, L., Skovronsky, D.M., Investigators, B.-., 2021. Effect of bamlanivimab vs placebo on incidence of COVID-19 among residents and staff of skilled nursing and assisted living facilities: a randomized clinical trial. JAMA 326, 46–55. https://doi.org/10.1001/jama.2021.8828.

Corman, V.M., Landt, O., Kaiser, M., Molenkamp, R., Meijer, A., Chu, D.K., Bleicker, T., Brünink, S., Schneider, J., Schmidt, M.L., Mulders, D.G., Haagmans, B.L., van der Veer, B., van den Brink, S., Wijsman, L., Goderski, G., Romette, J.L., Ellis, J., Zambon, M., Peiris, M., Goossens, H., Reusken, C., Koopmans, M.P., Drosten, C., 2020. Detection of 2019 novel coronavirus (2019-nCoV) by real-time RT-PCR. Euro Surveill. : bulletin Europeen sur les maladies transmissibles = European

communicable disease bulletin 25. https://doi.org/10.2807/1560-7917.es.2020.25.3.2000045.
Corti, D., Purcell, L.A., Snell, G., Veesler, D., 2021. Tackling COVID-19 with neutralizing monoclonal antibodies. Cell 184, 3086–3108. https://doi.org/10.1016/j.cell.2021.05.005.
Cox, M., Peacock, T.P., Harvey, W.T., Hughes, J., Wright, D.W., Willett, B.J., Thomson, E., Gupta, R.K., Peacock, S.J., Robertson, D.L., Carabelli, A.M., Consortium, C.-G.U., 2023. SARS-CoV-2 variant evasion of monoclonal antibodies based on in vitro studies. Nat. Rev. Microbiol. 21, 112–124. https://doi.org/10.1038/s41579-022-00809-7.
Dadonaite, B., Crawford, K.H.D., Radford, C.E., Farrell, A.G., Yu, T.C., Hannon, W.W., Zhou, P., Andrabi, R., Burton, D.R., Liu, L., Ho, D.D., Chu, H.Y., Neher, R.A., Bloom, J.D., 2023. A pseudovirus system enables deep mutational scanning of the full SARS-CoV-2 spike. Cell 186, 1263–1278.e1220. https://doi.org/10.1016/j.cell.2023.02.001.
Dejnirattisai, W., Huo, J., Zhou, D., Zahradník, J., Supasa, P., Liu, C., Duyvesteyn, H.M.E., Ginn, H.M., Mentzer, A.J., Tuekprakhon, A., Nutalai, R., Wang, B., Dijokaite, A., Khan, S., Avinoam, O., Bahar, M., Skelly, D., Adele, S., Johnson, S.A., Amini, A., Ritter, T.G., Mason, C., Dold, C., Pan, D., Assadi, S., Bellass, A., Omo-Dare, N., Koeckerling, D., Flaxman, A., Jenkin, D., Aley, P.K., Voysey, M., Costa Clemens, S.A., Naveca, F.G., Nascimento, V., Nascimento, F., Fernandes da Costa, C., Resende, P.C., Pauvolid-Correa, A., Siqueira, M.M., et al., 2022. SARS-CoV-2 Omicron-B.1.1.529 leads to widespread escape from neutralizing antibody responses. Cell 185, 467–484.e415. https://doi.org/10.1016/j.cell.2021.12.046.
del Rio, C., Malani, P.N., 2023. COVID-19 in the fall of 2023—forgotten but not gone. JAMA 330, 1517–1518. https://doi.org/10.1001/jama.2023.19049.
Dong, J., Zost, S.J., Greaney, A.J., Starr, T.N., Dingens, A.S., Chen, E.C., Chen, R.E., Case, J.B., Sutton, R.E., Gilchuk, P., Rodriguez, J., Armstrong, E., Gainza, C., Nargi, R.S., Binshtein, E., Xie, X., Zhang, X., Shi, P.-Y., Logue, J., Weston, S., McGrath, M.E., Frieman, M.B., Brady, T., Tuffy, K.M., Bright, H., Loo, Y.-M., McTamney, P.M., Esser, M.T., Carnahan, R.H., Diamond, M.S., Bloom, J.D., Crowe, J.E., 2021. Genetic and structural basis for SARS-CoV-2 variant neutralization by a two-antibody cocktail. Nature Microbiology 6, 1233–1244. https://doi.org/10.1038/s41564-021-00972-2.
ECDC, 2024. SARS-CoV-2 variants of concern as of 16 February 2024. https://www.ecdc.europa.eu/en/covid-19/variants-concern.
FDA, 2021. Coronavirus (COVID-19) update: FDA revokes emergency use authorization for monoclonal antibody bamlanivimab. https://www.fda.gov/news-events/press-announcements/coronavirus-covid-19-update-fda-revokes-emergency-use-authorization-monoclonal-antibody-bamlanivimab.
FDA, 2023a. Fact sheet for healthcare providers: emergency use authorization for Evusheld™ (tixagevimab co-packaged with cilgavimab). https://www.fda.gov/media/154701/download.
FDA, 2023b. Fact sheet for healthcare providers: emergency use authorization for Lagevrio™ (molnupiravir) capsules. https://www.fda.gov/media/155054/download.
FDA, 2023c. Fact sheet for healthcare providers: emergency use authorization for Sotrovimab. https://www.fda.gov/media/149534/download.
FDA, 2024. Emergency use authorizations for drugs and non-vaccine biological products. https://www.fda.gov/drugs/emergency-preparedness-drugs/emergency-use-authorizations-drugs-and-non-vaccine-biological-products.
Focosi, D., Casadevall, A., 2022. A critical analysis of the use of cilgavimab plus tixagevimab monoclonal antibody cocktail (Evusheld™) for COVID-19 prophylaxis and treatment. Viruses 14 (1999), 10.3390/v14091999.
Focosi, D., Casadevall, A., Franchini, M., Maggi, F., 2024. Sotrovimab: a review of its efficacy against SARS-CoV-2 variants. Viruses 16. https://doi.org/10.3390/v16020217.
Focosi, D., McConnell, S., Casadevall, A., Cappello, E., Valdiserra, G., Tuccori, M., 2022. Monoclonal antibody therapies against SARS-CoV-2. Lancet Infect. Dis. 22, e311–e326. https://doi.org/10.1016/s1473-3099(22)00311-5.
Francino-Urdaniz, I.M., Steiner, P.J., Kirby, M.B., Zhao, F., Haas, C.M., Barman, S., Rhodes, E.R., Leonard, A.C., Peng, L., Sprenger, K.G., Jardine, J.G., Whitehead, T.A., 2021. One-shot identification of SARS-CoV-2 S RBD escape mutants using yeast screening. Cell Rep. 36, 109627 https://doi.org/10.1016/j.celrep.2021.109627.
Gal-Tanamy, M., Keck, Z.-Y., Yi, M., McKeating, J.A., Patel, A.H., Foung, S.K.H., Lemon, S.M., 2008. In Vitro Selection of a Neutralization-Resistant Hepatitis C Virus Escape Mutant, 105. Proceedings of the National Academy of Sciences, pp. 19450–19455. https://doi.org/10.1073/pnas.0809879105.
Gangavarapu, K., Latif, A.A., Mullen, J.L., Alkuzweny, M., Hufbauer, E., Tsueng, G., Haag, E., Zeller, M., Aceves, C.M., Zaiets, K., Cano, M., Zhou, X., Qian, Z., Sattler, R., Matteson, N.L., Levy, J.I., Lee, R.T.C., Freitas, L., Maurer-Stroh, S., Suchard, M.A., Wu, C., Su, A.I., Andersen, K.G., Hughes, L.D., Core, G., Curation, T., 2023. Outbreak.info genomic reports: scalable and dynamic surveillance of SARS-CoV-2 variants and mutations. Nat. Methods 20, 512–522. https://doi.org/10.1038/s41592-023-01769-3.
Garrison, E., Kronenberg, Z.N., Dawson, E.T., Pedersen, B.S., Prins, P., 2022. A spectrum of free software tools for processing the VCF variant call format: vcflib, bio-vcf, cyvcf2, hts-nim and slivar. PLoS Comput. Biol. 18, e1009123 https://doi.org/10.1371/journal.pcbi.1009123.
Garrison, E.P., Marth, G.T., 2012. Haplotype-based variant detection from short-read sequencing. arXiv:1207.3907v2. https://doi.org/10.48550/ARXIV.1207.3907.
GISAID, 2024. Lineage comparison. https://gisaid.org/lineage-comparison/.
Guigon, A., Faure, E., Lemaire, C., Chopin, M.-C., Tinez, C., Assaf, A., Lazrek, M., Hober, D., Bocket, L., Engelmann, I., Alidjinou, E.K., 2022. Emergence of Q493R mutation in SARS-CoV-2 spike protein during bamlanivimab/etesevimab treatment and resistance to viral clearance. J. Infect. 84, 248–288. https://doi.org/10.1016/j.jinf.2021.08.033.
Gupta, A., Gonzalez-Rojas, Y., Juarez, E., Crespo Casal, M., Moya, J., Falci, D.R., Sarkis, E., Solis, J., Zheng, H., Scott, N., Cathcart, A.L., Hebner, C.M., Sager, J., Mogalian, E., Tipple, C., Peppercorn, A., Alexander, E., Pang, P.S., Free, A., Brinson, C., Aldinger, M., Shapiro, A.E., 2021. Early treatment for covid-19 with SARS-CoV-2 neutralizing antibody Sotrovimab. N. Engl. J. Med. 385, 1941–1950. https://doi.org/10.1056/NEJMoa2107934.
Haars, J., Palanisamy, N., Wallin, F., Molling, P., Lindh, J., Sundqvist, M., Ellstrom, P., Kaden, R., Lennerstrand, J., 2023. Prevalence of SARS-CoV-2 omicron sublineages and spike protein mutations conferring resistance against monoclonal antibodies in a Swedish cohort during 2022-2023. Microorganisms 11. https://doi.org/10.3390/microorganisms11102417.
Hoffmann, M., Hofmann-Winkler, H., Krüger, N., Kempf, A., Nehlmeier, I., Graichen, L., Arora, P., Sidarovich, A., Moldenhauer, A.-S., Winkler, M.S., Schulz, S., Jäck, H.-M., Stankov, M.V., Behrens, G.M.N., Pöhlmann, S., 2021. SARS-CoV-2 variant B.1.617 is resistant to bamlanivimab and evades antibodies induced by infection and vaccination. Cell Rep. 36, 109415 https://doi.org/10.1016/j.celrep.2021.109415.
Hoffmann, M., Kleine-Weber, H., Pöhlmann, S., 2020. A multibasic cleavage site in the spike protein of SARS-CoV-2 is essential for infection of human lung cells. Mol. Cell 78, 779–784.e775. https://doi.org/10.1016/j.molcel.2020.04.022.
Iketani, S., Liu, L., Guo, Y., Liu, L., Chan, J.F.W., Huang, Y., Wang, M., Luo, Y., Yu, J., Chu, H., Chik, K.K.H., Yuen, T.T.T., Yin, M.T., Sobieszczyk, M.E., Huang, Y., Yuen, K.-Y., Wang, H.H., Sheng, Z., Ho, D.D., 2022. Antibody evasion properties of SARS-CoV-2 Omicron sublineages. Nature 604, 553–556. https://doi.org/10.1038/s41586-022-04594-4.
Jackson, C.B., Farzan, M., Chen, B., Choe, H., 2022. Mechanisms of SARS-CoV-2 entry into cells. Nat. Rev. Mol. Cell Biol. 23, 3–20. https://doi.org/10.1038/s41580-021-00418-x.
Janion, C., Glickman, B.W., 1980. N4-hydroxycytidine: a mutagen specific for at to GC transitions. Mutat. Res. Fund Mol. Mech. Mutagen 72, 43–47. https://doi.org/10.1016/0027-5107(80)90218-3.
Jensen, B., Luebke, N., Feldt, T., Keitel, V., Brandenburger, T., Kindgen-Milles, D., Lutterbeck, M., Freise, N.F., Schoeler, D., Haas, R., Dilthey, A., Adams, O., Walker, A., Timm, J., Luedde, T., 2021. Emergence of the E484K mutation in SARS-COV-2-infected immunocompromised patients treated with bamlanivimab in Germany. The Lancet Regional Health - Europe 8, 100164. https://doi.org/10.1016/j.lanepe.2021.100164.
Johnson, B.A., Xie, X., Bailey, A.L., Kalveram, B., Lokugamage, K.G., Muruato, A., Zou, J., Zhang, X., Juelich, T., Smith, J.K., Zhang, L., Bopp, N., Schindewolf, C., Vu, M., Vanderheiden, A., Winkler, E.S., Swetnam, D., Plante, J.A., Aguilar, P., Plante, K.S., Popov, V., Lee, B., Weaver, S.C., Suthar, M.S., Routh, A.L., Ren, P., Ku, Z., An, Z., Debbink, K., Diamond, M.S., Shi, P.-Y., Freiberg, A.N., Menachery, V.D., 2021. Loss of furin cleavage site attenuates SARS-CoV-2 pathogenesis. Nature 591, 293–299. https://doi.org/10.1038/s41586-021-03237-4.
Johnson, M.C., Lyddon, T.D., Suarez, R., Salcedo, B., LePique, M., Graham, M., Ricana, C., Robinson, C., Ritter, D.G., 2020. Optimized pseudotyping conditions for the SARS-COV-2 spike glycoprotein. J. Virol. 94 https://doi.org/10.1128/JVI.01062-20.
Jones, B.E., Brown-Augsburger, P.L., Corbett, K.S., Westendorf, K., Davies, J., Cujec, T.P., Wiethoff, C.M., Blackbourne, J.L., Heinz, B.A., Foster, D., Higgs, R.E., Balasubramaniam, D., Wang, L., Zhang, Y., Yang, E.S., Bidshahri, R., Kraft, L., Hwang, Y., Žentelis, S., Jepson, K.R., Goya, R., Smith, M.A., Collins, D.W., Hinshaw, S.J., Tycho, S.A., Pellacani, D., Xiang, P., Muthuraman, K., Sobhanifar, S., Piper, M.H., Triana, F.J., Hendle, J., Pustilnik, A., Adams, A.C., Berens, S.J., Baric, R.S., Martinez, D.R., Cross, R.W., Geisbert, T.W., Borisevich, V., et al., 2021. The neutralizing antibody, LY-CoV555, protects against SARS-CoV-2 infection in nonhuman primates. Sci. Transl. Med. 13, eabf1906 https://doi.org/10.1126/scitranslmed.abf1906.
Kabinger, F., Stiller, C., Schmitzova, J., Dienemann, C., Kokic, G., Hillen, H.S., Hobartner, C., Cramer, P., 2021. Mechanism of molnupiravir-induced SARS-CoV-2 mutagenesis. Nat. Struct. Mol. Biol. 28, 740–746. https://doi.org/10.1038/s41594-021-00651-0.
Keam, S.J., 2022. Tixagevimab + cilgavimab: first approval. Drugs 82, 1001–1010. https://doi.org/10.1007/s40265-022-01731-1.
Khatri, R., Siddqui, G., Sadhu, S., Maithil, V., Vishwakarma, P., Lohiya, B., Goswami, A., Ahmed, S., Awasthi, A., Samal, S., 2023. Intrinsic D614G and P681R/H mutations in SARS-CoV-2 VoCs Alpha, Delta, Omicron and viruses with D614G plus key signature mutations in spike protein alters fusogenicity and infectivity. Med. Microbiol. Immunol. 212, 103–122. https://doi.org/10.1007/s00430-022-00760-7.
Lan, J., Ge, J., Yu, J., Shan, S., Zhou, H., Fan, S., Zhang, Q., Shi, X., Wang, Q., Zhang, L., Wang, X., 2020. Structure of the SARS-CoV-2 spike receptor-binding domain bound to the ACE2 receptor. Nature 581, 215–220. https://doi.org/10.1038/s41586-020-2180-5.
Langmead, B., Salzberg, S.L., 2012. Fast gapped-read alignment with Bowtie 2. Nat. Methods 9, 357–359. https://doi.org/10.1038/nmeth.1923.
Li, H., Durbin, R., 2009. Fast and accurate short read alignment with Burrows-Wheeler transform. Bioinformatics 25, 1754–1760. https://doi.org/10.1093/bioinformatics/btp324.
Li, H., Handsaker, B., Wysoker, A., Fennell, T., Ruan, J., Homer, N., Marth, G., Abecasis, G., Durbin, R., 2009. The sequence alignment/map format and SAMtools. Bioinformatics 25, 2078–2079. https://doi.org/10.1093/bioinformatics/btp352.
Li, P., Wang, Y., Lavrijsen, M., Lamers, M.M., de Vries, A.C., Rottier, R.J., Bruno, M.J., Peppelenbosch, M.P., Haagmans, B.L., Pan, Q., 2022. SARS-CoV-2 Omicron variant is highly sensitive to molnupiravir, nirmatrelvir, and the combination. Cell Res. 32, 322–324. https://doi.org/10.1038/s41422-022-00618-w.

Loo, Y.-M., McTamney, P.M., Arends, R.H., Abram, M.E., Aksyuk, A.A., Diallo, S., Flores, D.J., Kelly, E.J., Ren, K., Roque, R., Rosenthal, K., Streicher, K., Tuffy, K.M., Bond, N.J., Cornwell, O., Bouquet, J., Cheng, L.I., Dunyak, J., Huang, Y., Rosenbaum, A.I., Pilla Reddy, V., Andersen, H., Carnahan, R.H., Crowe, J.E., Kuehne, A.I., Herbert, A.S., Dye, J.M., Bright, H., Kallewaard, N.L., Pangalos, M.N., Esser, M.T., 2022. The SARS-CoV-2 monoclonal antibody combination, AZD7442, is protective in nonhuman primates and has an extended half-life in humans. Sci. Transl. Med. 14, eabl8124 https://doi.org/10.1126/scitranslmed.abl8124.

Lupala, C.S., Ye, Y., Chen, H., Su, X.-D., Liu, H., 2022. Mutations on RBD of SARS-CoV-2 Omicron variant result in stronger binding to human ACE2 receptor. Biochem. Biophys. Res. Commun. 590, 34–41. https://doi.org/10.1016/j.bbrc.2021.12.079.

Mannar, D., Saville, J.W., Zhu, X., Srivastava, S.S., Berezuk, A.M., Tuttle, K.S., Marquez, A.C., Sekirov, I., Subramaniam, S., 2022. SARS-CoV-2 Omicron variant: antibody evasion and cryo-EM structure of spike protein–ACE2 complex. Science (New York, N.Y.) 375, 760–764. https://doi.org/10.1126/science.abn7760.

Martin, M., 2011. Cutadapt removes adapter sequences from high-throughput sequencing reads. EMBnet.journal 17, 10. https://doi.org/10.14806/ej.17.1.200.

Mia, M.E., Howlader, M., Akter, F., Hossain, M.M., 2024. Preclinical and clinical investigations of potential drugs and vaccines for COVID-19 therapy: a comprehensive review with recent update. Clinical Pathology 17, 2632010X241263054. https://doi.org/10.1177/2632010x241263054.

Moeller, N.H., Shi, K., Demir, Ö., Belica, C., Banerjee, S., Yin, L., Durfee, C., Amaro, R.E., Aihara, H., 2022. Structure and dynamics of SARS-CoV-2 proofreading exoribonuclease ExoN. Proc. Natl. Acad. Sci. USA 119, e2106379119. https://doi.org/10.1073/pnas.2106379119.

Montgomery, H., Hobbs, F.D.R., Padilla, F., Arbetter, D., Templeton, A., Seegobin, S., Kim, K., Campos, J.A.S., Arends, R.H., Brodek, B.H., Brooks, D., Garbes, P., Jimenez, J., Koh, G.C.K.W., Padilla, K.W., Streicher, K., Viani, R.M., Alagappan, V., Pangalos, M.N., Esser, M.T., 2022. Efficacy and safety of intramuscular administration of tixagevimab–cilgavimab for early outpatient treatment of COVID-19 (TACKLE): a phase 3, randomised, double-blind, placebo-controlled trial. Lancet Respir. Med. 10, 985–996. https://doi.org/10.1016/S2213-2600(22)00180-1.

NCBI, 2023. SARS-CoV-2 variants overview. https://www.ncbi.nlm.nih.gov/activ/help#downloadAllData.

Oladunni, F.S., Park, J.-G., Chiem, K., Ye, C., Pipenbrink, M., Walter, M.R., Kobie, J., Martinez-Sobrido, L., 2021. Selection, identification, and characterization of SARS-CoV-2 monoclonal antibody resistant mutants. J. Virol Methods 290, 114084. https://doi.org/10.1016/j.jviromet.2021.114084.

Pandey, L.K., Mohapatra, J.K., Subramaniam, S., Sanyal, A., Pande, V., Pattnaik, B., 2014. Evolution of serotype A foot-and-mouth disease virus capsid under neutralizing antibody pressure in vitro. Virus Res. 181, 72–76. https://doi.org/10.1016/j.virusres.2014.01.009.

Park, Y.-J., De Marco, A., Starr, T.N., Liu, Z., Pinto, D., Walls, A.C., Zatta, F., Zepeda, S.K., Bowen, J.E., Sprouse, K.R., Joshi, A., Giurdanella, M., Guarino, B., Noack, J., Abdelnabi, R., Foo, S.-Y.C., Rosen, L.E., Lempp, F.A., Benigni, F., Snell, G., Neyts, J., Whelan, S.P.J., Virgin, H.W., Bloom, J.D., Corti, D., Pizzuto, M.S., Veesler, D., 2022. Antibody-mediated broad sarbecovirus neutralization through ACE2 molecular mimicry. Science (New York, N.Y.) 375, 449–454. https://doi.org/10.1126/science.abm8143.

Pastorio, C., Zech, F., Noettger, S., Jung, C., Jacob, T., Sanderson, T., Sparrer, K.M.J., Kirchhoff, F., 2022. Determinants of Spike infectivity, processing, and neutralization in SARS-CoV-2 Omicron subvariants BA.1 and BA.2. Cell Host Microbe 30, 1255–1268.e1255. https://doi.org/10.1016/j.chom.2022.07.006.

Peacock, T.P., Goldhill, D.H., Zhou, J., Baillon, L., Frise, R., Swann, O.C., Kugathasan, R., Penn, R., Brown, J.C., Sanchez-David, R.Y., Braga, L., Williamson, M.K., Hassard, J. A., Staller, E., Hanley, B., Osborn, M., Giacca, M., Davidson, A.D., Matthews, D.A., Barclay, W.S., 2021. The furin cleavage site in the SARS-CoV-2 spike protein is required for transmission in ferrets. Nature Microbiology 6, 899–909. https://doi.org/10.1038/s41564-021-00908-w.

Pinto, D., Park, Y.-J., Beltramello, M., Walls, A.C., Tortorici, M.A., Bianchi, S., Jaconi, S., Culap, K., Zatta, F., De Marco, A., Peter, A., Guarino, B., Spreafico, R., Cameroni, E., Case, J.B., Chen, R.E., Havenar-Daughton, C., Snell, G., Telenti, A., Virgin, H.W., Lanzavecchia, A., Diamond, M.S., Fink, K., Veesler, D., Corti, D., 2020. Cross-neutralization of SARS-CoV-2 by a human monoclonal SARS-CoV antibody. Nature 583, 290–295. https://doi.org/10.1038/s41586-020-2349-y.

Ragonnet-Cronin, M., Nutalai, R., Huo, J., Dijokaite-Guraliuc, A., Das, R., Tuekprakhon, A., Supasa, P., Liu, C., Selvaraj, M., Groves, N., Hartman, H., Ellaby, N., Mark Sutton, J., Bahar, M.W., Zhou, D., Fry, E., Ren, J., Brown, C., Klenerman, P., Dunachie, S.J., Mongkolsapaya, J., Hopkins, S., Chand, M., Stuart, D. I., Screaton, G.R., Rokadiya, S., 2023. Generation of SARS-CoV-2 escape mutations by monoclonal antibody therapy. Nat. Commun. 14, 3334. https://doi.org/10.1038/s41467-023-37826-w.

Razonable, R.R., Tulledge-Scheitel, S.M., Hanson, S.N., Arndt, R.F., Speicher, L.L., Seville, T.A., Larsen, J.J., Ganesh, R., O'Horo, J.C., 2022. Real-world clinical outcomes of bebtelovimab and Sotrovimab treatment of high-risk persons with coronavirus disease 2019 during the omicron epoch. Open Forum Infect. Dis. 9, ofac411. https://doi.org/10.1093/ofid/ofac411.

Reynard, O., Nguyen, X.N., Alazard-Dany, N., Barateau, V., Cimarelli, A., Volchkov, V.E., 2015. Identification of a new ribonucleoside inhibitor of ebola virus replication. Viruses 7, 6233–6240. https://doi.org/10.3390/v7122934.

Robson, F., Khan, K.S., Le, T.K., Paris, C., Demirbag, S., Barfuss, P., Rocchi, P., Ng, W.-L., 2020. Coronavirus RNA proofreading: molecular basis and therapeutic targeting. Mol. Cell 79, 710–727. https://doi.org/10.1016/j.molcel.2020.07.027.

Rockett, R., Basile, K., Maddocks, S., Fong, W., Agius, J.E., Johnson-Mackinnon, J., Arnott, A., Chandra, S., Gall, M., Draper, J., Martinez, E., Sim, E.M., Lee, C., Ngo, C., Ramsperger, M., Ginn, A.N., Wang, Q., Fennell, M., Ko, D., Lim, H.L., Gilroy, N., O'Sullivan, M.V.N., Chen, S.C., Kok, J., Dwyer, D.E., Sintchenko, V., 2022. Resistance mutations in SARS-CoV-2 Delta variant after Sotrovimab use. N. Engl. J. Med. 386, 1477–1479. https://doi.org/10.1056/NEJMc2120219.

Ruden, D.M., Cingolani, P., Patel, V.M., Coon, M., Nguyen, T., Land, S.J., Lu, X., 2012. Using Drosophila melanogaster as a model for genotoxic chemical mutational studies with a new program, SnpSift. Front. Genet. 3 https://doi.org/10.3389/fgene.2012.00035.

Schrodinger, L.L.C., 2015. The PyMOL Molecular Graphics System, Version 1.8.

Scialo, F., Daniele, A., Amato, F., Pastore, L., Matera, M.G., Cazzola, M., Castaldo, G., Bianco, A., 2020. ACE2: the major cell entry receptor for SARS-CoV-2. Lung 198, 867–877. https://doi.org/10.1007/s00408-020-00408-4.

Shah, M., Woo, H.G., 2022. Omicron: a heavily mutated SARS-CoV-2 variant exhibits stronger binding to ACE2 and potently escapes approved COVID-19 therapeutic antibodies. Front. Immunol. 12 https://doi.org/10.3389/fimmu.2021.830527.

Sharma, D., Rawat, P., Greiff, V., Janakiraman, V., Gromiha, M.M., 2024. Predicting the immune escape of SARS-CoV-2 neutralizing antibodies upon mutation. Biochim. Biophys. Acta (BBA) - Mol. Basis Dis. 1870, 166959 https://doi.org/10.1016/j.bbadis.2023.166959.

Sheahan, T.P., Sims, A.C., Zhou, S., Graham, R.L., Pruijssers, A.J., Agostini, M.L., Leist, S. R., Schafer, A., Dinnon 3rd, K.H., Stevens, L.J., Chappell, J.D., Lu, X., Hughes, T.M., George, A.S., Hill, C.S., Montgomery, S.A., Brown, A.J., Bluemling, G.R., Natchus, M. G., Saindane, M., Kolykhalov, A.A., Painter, G., Harcourt, J., Tamin, A., Thornburg, N.J., Swanstrom, R., Denison, M.R., Baric, R.S., 2020. An orally bioavailable broad-spectrum antiviral inhibits SARS-CoV-2 in human airway epithelial cell cultures and multiple coronaviruses in mice. Sci. Transl. Med. 12 https://doi.org/10.1126/scitranslmed.abb5883.

Shruti, K., Céline, G., Lucas, F., Mark, B.S., Gunter, B., Amadou, D., Nancy, A., Joses, H., Raphael, T.C.L., Winston, Y., Team, G.C.C., Sebastian, M.-S., 2021. GISAID's Role in Pandemic Response, 3, pp. 1049–1051. https://doi.org/10.46234/ccdcw2021.255.

Sidarovich, A., Krüger, N., Rocha, C., Graichen, L., Kempf, A., Nehlmeier, I., Lier, M., Cossmann, A., Stankov, M.V., Schulz, S.R., Behrens, G.M.N., Jäck, H.-M., Pöhlmann, S., Hoffmann, M., 2022. Host cell entry and neutralization sensitivity of SARS-CoV-2 lineages B.1.620 and R.1. Viruses 14, 2475.

Starr, T.N., Czudnochowski, N., Liu, Z., Zatta, F., Park, Y.-J., Addetia, A., Pinto, D., Beltramello, M., Hernandez, P., Greaney, A.J., Marzi, R., Glass, W.G., Zhang, I., Dingens, A.S., Bowen, J.E., Tortorici, M.A., Walls, A.C., Wojcechowskyj, J.A., De Marco, A., Rosen, L.E., Zhou, J., Montiel-Ruiz, M., Kaiser, H., Dillen, J.R., Tucker, H., Bassi, J., Silacci-Fregni, C., Housley, M.P., di Iulio, J., Lombardo, G., Agostini, M., Sprugasci, N., Culap, K., Jaconi, S., Meury, M., Dellota Jr., E., Abdelnabi, R., Foo, S.-Y.C., Cameroni, E., Stumpf, S., et al., 2021a. SARS-CoV-2 RBD antibodies that maximize breadth and resistance to escape. Nature 597, 97–102. https://doi.org/10.1038/s41586-021-03807-6.

Starr, T.N., Greaney, A.J., Dingens, A.S., Bloom, J.D., 2021b. Complete map of SARS-CoV-2 RBD mutations that escape the monoclonal antibody LY-CoV555 and its cocktail with LY-CoV016. Cell Reports Medicine 2, 100255. https://doi.org/10.1016/j.xcrm.2021.100255.

Stegmann, K.M., Dickmanns, A., Gerber, S., Nikolova, V., Klemke, L., Manzini, V., Schlösser, D., Bierwirth, C., Freund, J., Sitte, M., Lugert, R., Salinas, G., Meister, T.L., Pfaender, S., Görlich, D., Wollnik, B., Groß, U., Dobbelstein, M., 2021. The folate antagonist methotrexate diminishes replication of the coronavirus SARS-CoV-2 and enhances the antiviral efficacy of remdesivir in cell culture models. Virus Res. 302, 198469 https://doi.org/10.1016/j.virusres.2021.198469.

Syed, Y.Y., 2022. Molnupiravir: first approval. Drugs 82, 455–460. https://doi.org/10.1007/s40265-022-01684-5.

Taft, J.M., Weber, C.R., Gao, B., Ehling, R.A., Han, J., Frei, L., Metcalfe, S.W., Overath, M.D., Yermanos, A., Kelton, W., Reddy, S.T., 2022. Deep mutational learning predicts ACE2 binding and antibody escape to combinatorial mutations in the SARS-CoV-2 receptor-binding domain. Cell 185, 4008–4022.e4014. https://doi.org/10.1016/j.cell.2022.08.024.

Takashita, E., Kinoshita, N., Yamayoshi, S., Sakai-Tagawa, Y., Fujisaki, S., Ito, M., Iwatsuki-Horimoto, K., Chiba, S., Halfmann, P., Nagai, H., Saito, M., Adachi, E., Sullivan, D., Pekosz, A., Watanabe, S., Maeda, K., Imai, M., Yotsuyanagi, H., Mitsuya, H., Ohmagari, N., Takeda, M., Hasegawa, H., Kawaoka, Y., 2022. Efficacy of antibodies and antiviral drugs against covid-19 omicron variant. N. Engl. J. Med. 386, 995–998. https://doi.org/10.1056/NEJMc2119407.

Thomson, E.C., Rosen, L.E., Shepherd, J.G., Spreafico, R., da Silva Filipe, A., Wojcechowskyj, J.A., Davis, C., Piccoli, L., Pascall, D.J., Dillen, J., Lytras, S., Czudnochowski, N., Shah, R., Meury, M., Jesudason, N., De Marco, A., Li, K., Bassi, J., O'Toole, A., Pinto, D., Colquhoun, R.M., Culap, K., Jackson, B., Zatta, F., Rambaut, A., Jaconi, S., Sreenu, V.B., Nix, J., Zhang, I., Jarrett, R.F., Glass, W.G., Beltramello, M., Nomikou, K., Pizzuto, M., Tong, L., Cameroni, E., Croll, T.I., Johnson, N., Di Iulio, J., Wickenhagen, A., et al., 2021. Circulating SARS-CoV-2 spike N439K variants maintain fitness while evading antibody-mediated immunity. Cell 184, 1171–1187.e1120. https://doi.org/10.1016/j.cell.2021.01.037.

Toots, M., Yoon, J.J., Cox, R.M., Hart, M., Sticher, Z.M., Makhsous, N., Plesker, R., Barrena, A.H., Reddy, P.G., Mitchell, D.G., Shean, R.C., Bluemling, G.R., Kolykhalov, A.A., Greninger, A.L., Natchus, M.G., Painter, G.R., Plemper, R.K., 2019. Characterization of orally efficacious influenza drug with high resistance barrier in ferrets and human airway epithelia. Sci. Transl. Med. 11 https://doi.org/10.1126/scitranslmed.aax5866.

Urakova, N., Kuznetsova, V., Crossman, D.K., Sokratian, A., Guthrie, D.B., Kolykhalov, A. A., Lockwood, M.A., Natchus, M.G., Crowley, M.R., Painter, G.R., Frolova, E.I., Frolov, I., 2018. beta-d-N(4)-Hydroxycytidine is a potent anti-alphavirus compound that induces a high level of mutations in the viral genome. J. Virol. 92 https://doi.org/10.1128/JVI.01965-17.

VanBlargan, L.A., Errico, J.M., Halfmann, P.J., Zost, S.J., Crowe, J.E., Purcell, L.A., Kawaoka, Y., Corti, D., Fremont, D.H., Diamond, M.S., 2022. An infectious SARS-CoV-2 B.1.1.529 Omicron virus escapes neutralization by therapeutic monoclonal antibodies. Nat. Med. 28, 490–495. https://doi.org/10.1038/s41591-021-01678-y.

Vellas, C., Kamar, N., Izopet, J., 2022. Resistance mutations in SARS-CoV-2 omicron variant after tixagevimab-cilgavimab treatment. J. Infect. 85, e162–e163. https://doi.org/10.1016/j.jinf.2022.07.014.

Wang, Q., Iketani, S., Li, Z., Liu, L., Guo, Y., Huang, Y., Bowen, A.D., Liu, M., Wang, M., Yu, J., Valdez, R., Lauring, A.S., Sheng, Z., Wang, H.H., Gordon, A., Liu, L., Ho, D.D., 2023a. Alarming antibody evasion properties of rising SARS-CoV-2 BQ and XBB subvariants. Cell 186, 279–286.e278. https://doi.org/10.1016/j.cell.2022.12.018.

Wang, Q., Ye, S.B., Zhou, Z.J., Song, A.L., Zhu, X., Peng, J.M., Liang, R.M., Yang, C.H., Yu, X.W., Huang, X., Yu, J., Qiu, Y., Ge, X.Y., 2023b. Key mutations in the spike protein of SARS-CoV-2 affecting neutralization resistance and viral internalization. J. Med. Virol. 95, e28407 https://doi.org/10.1002/jmv.28407.

Wang, Y., Yan, A., Song, D., Duan, M., Dong, C., Chen, J., Jiang, Z., Gao, Y., Rao, M., Feng, J., Zhang, Z., Qi, R., Ma, X., Liu, H., Yu, B., Wang, Q., Zong, M., Jiao, J., Xing, P., Pan, R., Li, D., Xiao, J., Sun, J., Li, Y., Zhang, L., Shen, Z., Sun, B., Zhao, Y., Zhang, L., Dai, J., Zhao, J., Wang, L., Dou, C., Liu, Z., Zhao, J., 2024. Identification of a highly conserved neutralizing epitope within the RBD region of diverse SARS-CoV-2 variants. Nat. Commun. 15, 842. https://doi.org/10.1038/s41467-024-45050-3.

Westendorf, K., Žentelis, S., Wang, L., Foster, D., Vaillancourt, P., Wiggin, M., Lovett, E., van der Lee, R., Hendle, J., Pustilnik, A., Sauder, J.M., Kraft, L., Hwang, Y., Siegel, R. W., Chen, J., Heinz, B.A., Higgs, R.E., Kallewaard, N.L., Jepson, K., Goya, R., Smith, M.A., Collins, D.W., Pellacani, D., Xiang, P., de Puyraimond, V., Ricicova, M., Devorkin, L., Pritchard, C., O'Neill, A., Dalal, K., Panwar, P., Dhupar, H., Garces, F. A., Cohen, C.A., Dye, J.M., Huie, K.E., Badger, C.V., Kobasa, D., Audet, J., Freitas, J. J., et al., 2022. LY-CoV1404 (bebtelovimab) potently neutralizes SARS-CoV-2 variants. Cell Rep. 39, 110812 https://doi.org/10.1016/j.celrep.2022.110812.

Willett, B.J., Grove, J., MacLean, O.A., Wilkie, C., De Lorenzo, G., Furnon, W., Cantoni, D., Scott, S., Logan, N., Ashraf, S., Manali, M., Szemiel, A., Cowton, V., Vink, E., Harvey, W.T., Davis, C., Asamaphan, P., Smollett, K., Tong, L., Orton, R., Hughes, J., Holland, P., Silva, V., Pascall, D.J., Puxty, K., da Silva Filipe, A., Yebra, G., Shaaban, S., Holden, M.T.G., Pinto, R.M., Gunson, R., Templeton, K., Murcia, P.R., Patel, A.H., Klenerman, P., Dunachie, S., Consortium, P., Consortium, C.-G.U., Haughney, J., Robertson, D.L., et al., 2022. SARS-CoV-2 Omicron is an immune escape variant with an altered cell entry pathway. Nat Microbiol 7, 1161–1179. https://doi.org/10.1038/s41564-022-01143-7.

Wood, D.E., Salzberg, S.L., 2014. Kraken: ultrafast metagenomic sequence classification using exact alignments. Genome Biol. 15, R46. https://doi.org/10.1186/gb-2014-15-3-r46.

Xiao, T.S., Lu, J.M., Zhang, J., Johnson, R.I., McKay, L.G.A., Storm, N., Lavine, C.L., Peng, H.Q., Cai, Y.F., Rits-Volloch, S., Lu, S., Quinlan, B.D., Farzan, M., Seaman, M. S., Griffiths, A., Chen, B., 2021. A trimeric human angiotensin-converting enzyme 2 as an anti-SARS-CoV-2 agent. Nat. Struct. Mol. Biol. 28, 202. https://doi.org/10.1038/s41594-020-00549-3.

Yi, C., Sun, X., Lin, Y., Gu, C., Ding, L., Lu, X., Yang, Z., Zhang, Y., Ma, L., Gu, W., Qu, A., Zhou, X., Li, X., Xu, J., Ling, Z., Xie, Y., Lu, H., Sun, B., 2021. Comprehensive mapping of binding hot spots of SARS-CoV-2 RBD-specific neutralizing antibodies for tracking immune escape variants. Genome medicine 13, 164. https://doi.org/10.1186/s13073-021-00985-w.

Yin, W., Xu, Y., Xu, P., Cao, X., Wu, C., Gu, C., He, X., Wang, X., Huang, S., Yuan, Q., Wu, K., Hu, W., Huang, Z., Liu, J., Wang, Z., Jia, F., Xia, K., Liu, P., Wang, X., Song, B., Zheng, J., Jiang, H., Cheng, X., Jiang, Y., Deng, S.-J., Xu, H.E., 2022. Structures of the Omicron spike trimer with ACE2 and an anti-Omicron antibody. Science (New York, N.Y.) 375, 1048–1053. https://doi.org/10.1126/science.abn8863.

Zhang, L., Jackson, C.B., Mou, H., Ojha, A., Peng, H., Quinlan, B.D., Rangarajan, E.S., Pan, A., Vanderheiden, A., Suthar, M.S., Li, W., Izard, T., Rader, C., Farzan, M., Choe, H., 2020. SARS-CoV-2 spike-protein D614G mutation increases virion spike density and infectivity. Nat. Commun. 11, 6013. https://doi.org/10.1038/s41467-020-19808-4.

Zhao, Z., Zhou, J., Tian, M., Huang, M., Liu, S., Xie, Y., Han, P., Bai, C., Han, P., Zheng, A., Fu, L., Gao, Y., Peng, Q., Li, Y., Chai, Y., Zhang, Z., Zhao, X., Song, H., Qi, J., Wang, Q., Wang, P., Gao, G.F., 2022. Omicron SARS-CoV-2 mutations stabilize spike up-RBD conformation and lead to a non-RBM-binding monoclonal antibody escape. Nat. Commun. 13, 4958. https://doi.org/10.1038/s41467-022-32665-7.

Zibat, A., Zhang, X., Dickmanns, A., Stegmann, K.M., Dobbelstein, A.W., Alachram, H., Soliwoda, R., Salinas, G., Groß, U., Görlich, D., Kschischo, M., Wollnik, B., Dobbelstein, M., 2023. N4-hydroxycytidine, the active compound of Molnupiravir, promotes SARS-CoV-2 mutagenesis and escape from a neutralizing nanobody. iScience 26, 107786. https://doi.org/10.1016/j.isci.2023.107786.

Zimmer, G., Locher, S., Berger Rentsch, M., Halbherr, S.J., 2014. Pseudotyping of vesicular stomatitis virus with the envelope glycoproteins of highly pathogenic avian influenza viruses. J. Gen. Virol. 95, 1634–1639. https://doi.org/10.1099/vir.0.065201-0.

Zost, S.J., Gilchuk, P., Case, J.B., Binshtein, E., Chen, R.E., Nkolola, J.P., Schäfer, A., Reidy, J.X., Trivette, A., Nargi, R.S., Sutton, R.E., Suryadevara, N., Martinez, D.R., Williamson, L.E., Chen, E.C., Jones, T., Day, S., Myers, L., Hassan, A.O., Kafai, N.M., Winkler, E.S., Fox, J.M., Shrihari, S., Mueller, B.K., Meiler, J., Chandrashekar, A., Mercado, N.B., Steinhardt, J.J., Ren, K., Loo, Y.-M., Kallewaard, N.L., McCune, B.T., Keeler, S.P., Holtzman, M.J., Barouch, D.H., Gralinski, L.E., Baric, R.S., Thackray, L. B., Diamond, M.S., Carnahan, R.H., et al., 2020. Potently neutralizing and protective human antibodies against SARS-CoV-2. Nature 584, 443–449. https://doi.org/10.1038/s41586-020-2548-6.